Answers for Anonymous Referee #1

General Comments

This paper presents a 10-year radar-based climatology of hail frequency in a portion of western Europe encompassing France, Germany, Belgium and Luxembourg. The authors combine 2D reflectivity composites from the French and German weather services into a single mosaic with a resolution of 1 km 2 and then applying storm cell tracking with a 55 dBZ reflectivity threshold to identify likely hail events. The spatial distribution of hail is analysed, with particular focus on the relation to surface topography (coastlines and mountain ranges), along with diurnal and seasonal variations in different parts of the study domain. The authors also examine the characteristics of the identified cell tracks, including their length, width, duration, and orientation.

The length and spatial extent of this analysis alone make it a novel contribution to the hail climatology literature, which often focuses on smaller regions. The paper is largely well written and the figures are mostly of a high quality. However, I see a number of issues that need to be addressed before this work can be accepted for publication. Chief among these is the unacceptable amount of speculation in the results, particularly when it comes to discussion around the role of surface topography in hailstorm formation. I would also like to see more details regarding the construction of the national radar composites and discussion on the importance of radar calibration errors. Detailed comments are provided below.
#We thank again the reviewer for his report and suggestions. We deleted unjustified speculations and added a new section with the role of surface topography in hailstorm formation with a special emphasis on the Massif Central in France, which is the region the most affected by hail in our study. We also added a paragraph about the construction and quality control procedures of both French and German national radar composites.
All major and minor corrections suggested by the reviewer were addressed in the new manuscript and appear in blue in the corrected version.

Specific Comments

Major Comment 1:

Currently, your results section contains too much speculation, particularly when it comes to the role of surface topography in the formation of hail storms. Examples include L197-207, L223-226, and L249-253. It is fine to note the clear correspondence between high hail

frequencies and orographic features, but not to speculate at length on the underlying mechanisms in the absence of detailed observations or numerical simulations (either presented here or in other published studies). A bit of speculation is OK, but this should probably be reserved for the conclusions/discussion, where it can be used to motivate future investigation into physical mechanisms. Alternatively, if you do want to at least start this investigation here, you could use sounding or reanalysis data to examine the flow characteristics (wind speed and direction, Froude number, etc) on hail days in your various subdomains (c.f. section 6 of Kunz and Puskeiler 2010). This would obviously involve a bit of extra work (and additional data), but would make this study more than just "another hail climatology."

#We removed some speculations for example in Sections 4.1, 4.2 and 4.3. As we wanted to start the investigation about the wind flow, we computed the flow (direction and velocity at 10 m) during days with hail in mountainous area (near the Massif-Central, Pyrenees and Vosges in France; and nearby the Black-Forest and Ore Mountains in Germany). The Froude number was also calculated using ERA5 reanalysis that we overlapped on ETOPO1, a high-resolution global relief (1 arc-minute resolution). The low Froude numbers in all regions support the hypothesis of a predominant flow-around wind regime during hail days. In the reviewed manuscript version, an example is shown for the Massif Central only in Figure 4, and a detailed description of Figure 4 is following from Line 316 to Line 346 in the new manuscript version. Finally, we compared our results with some recent literature about hailstorms occurrence in the vicinity of topography in Europe; as well as convection initiation in complex terrain (now Lines 347 to 355).

Major Comment 2:

I'd like to see a bit more detail regarding how the French and German radar composites are produced. For example, do they use radar from the lower (or lowest unblocked) tilt only or do they compute a column-maximum reflectivity across all tilts? How are reflectivities combined in regions of overlapping coverage? Is the nearest radar used, the one with the lowest unblocked beam, or is a more complex quality index applied? Is any account taken for variations in beam diameter with range or differences in beam width between different radars? Such information is important for the reader to understand limitations in the composite product.

#We followed the suggestion of the reviewer by adding two detailed paragraphs, one for France (Lines 101 to 149) and another one for Germany (Lines 150 to 173), both of them including: 1. A short historic of the national radar network. 2. A description of individual radars (types of radar + brief geographical location + enumeration of radar changes + observation techniques). 3. A description of the national radar composite merging using individual radars. 4. Strategies adopted while considering regions with overlapping radar scans 5. Signal processing. 6. Quality-controls applied at each production step.

Major Comment 3:

Radar miscalibration is a major issue in many operational networks and can lead to significant inhomogeneities across large study domains. It is also a very tricky problem to overcome, although methods do exist (see, for example, Louf et al. 2019). However, for the purpose of this study I think you just need to mention it as a potential source of error in your results. Specifically, differences in radar calibration across the study domain may lead to an overestimation of the relative hail frequency in some regions (where radars are calibrated too high) and underestimation of the relative hail frequency in others (where radars are calibrated too low).

As suggested, we added more comments in the text about radar miscalibrations leading to data inhomogeinities (now Line 179 to Line 185).

Minor comments

L3: My first question on seeing the study period is why does it end six years ago in 2014? Was one (or both) of the national composites not available for later dates? This information should be provided in section 2.

#We added two sentences to explain that this study focuses on the first phase of the project HAMLET (Lines 90 and 91) where radar data from France where available until 2014 only. This is due to the installation of five new X-band radars in 2014 in the French radar composite requiring further calibrations and quality controls into the national radar composite.

L26-36: You should also mention radar-based hail climatologies from other parts of the world, such as the USA (Cinineo et al. 2012) and Australia (Soderholm et al. 2017, Warren et al. 2020).

We commented on additional radar-based hail climatologies from other parts of the world including the reviewer's literature suggestions (Lines 56 to 64).

L39: I would argue that the issue isn't that these satellite- and model-based methods are "not as straightforward as those based on radar reflectivity. Rather it is that the link between the observed quantities and hail occurrence at the surface is less direct than it is with radar-based measurements.

We changed this statement for "the link between the observed quantities and hail occurrence at the surface is less direct than with radar-based measurements".

L50: Your study provides information about the frequency of hail but not its intensity; as such this statement should be modified.

#We removed "intensity" from the sentence.

L53-54: Section 4 also presents results on seasonal and diurnal variations in hail frequency and the characteristics of the hail cells. Maybe mention this here.

#We added these statements in now Lines 85-87.

L64: Why 2015 when your study covers 2005-2014? If the number or type of radars changed during your study period this should be mentioned.
#We rephrased this sentence (Line 92).

L69-70: What map projection (coordinate system) does the French mosaic use?
#The French mosaics are available in Cartesian coordinates, as described on the website of the French Weather Service:

https://donneespubliques.meteofrance.fr/?fond=rubrique&id_rubrique=27

L72-73: This sentence needs rephrasing. What sort of quality checks are performed?
#We deleted this sentence. A strict protocol of quality checks is applied for both French and German national radar composites. We detailed the main quality check stages for the French radar composites in Lines 124 to 141. These steps are also described for the German radar composites from Line 159 to Line 167.

L76: Does this mean that there is a gap in the data from mid-June to late-July 2009? Are there any other gaps during the study period? These will need to be accounted for if you estimate annual hail frequencies, as recommended below.
#We modified this sentence in the new version of the manuscript (now line 146). There were no missing days without a radar national composite during the whole period from 2005 to 2014. Few local single-radar data might miss on very specific times but Météo-France did not report any major radar failures that could affect our climatology.

L77: Why did you bother processing the coarse resolution data from 1999 to 2004 when your study period only starts in 2005?
#We removed “1999” and change it for “2004”.

L80: Again, why discuss the state of the network in a year that falls outside your study period? How many radars were operational during 2005 to 2014 and did this number change?
#We only mention the years 2005 to 2014 in the reviewed version (line 150). During 2005 to 2014, one radar station was added in 2012 in Memmingen (South Germany). The number of radar did not changed during 2005 and 2014 for France but few radars were replaced. We added these assumption in L151-152 for Germany and in L103-114 for France.

L82-83: Figure 2 suggests that all of Germany is covered by the radar composite, with no gaps. The locations that you mention (the far north near the Danish border and southeastern Bavaria) are only covered by a single radar, but they will still surely feature in the composite.

#Looking at long-term radar composites, the far north place near the Danish border and the southeastern part of Bavaria have no reflectivity values; we rather see some values near the location of the radar stations. We added these sentences in L154-156.

L88-91: This type of data compression is quite common. Since the resolution of the data is quite high (0.5 dB) I don't think this needs to be discussed. It would only be worth mentioning if there were only a few reflectivity levels (as in Puskeiler et al. 2016).
#We deleted this statement.

L98: I'm not sure what you mean by the "standard coordinate system". What map projection is used? I'm guessing it differs from the ones used in the French and German composites.
Was any account taken of this difference? Given that each domain covers around 1000 km, there could be some distortions introduced in this procedure.
#Details about the coordinate system were added in L185-189. We used WGS84 as geographic coordinate system (EPSG code: 4326) with the following three properties: 1. Datum is set to WGS84 with a 6378137 m equatorial radius for the oblate ellipsoid at the equator and a flattening of 1/298.257223563. 2. The prime meridian is Greenwich. 3. Units are in degrees.
We used the software ArcGIS that by default plot a map with a Pseudo Plate Carree projection. In the revised version, all maps were projected to a Lambert Conformal Conic projection that best suit for mid-latitudes. An applied example of this projection can be find in Figure 3.

L113-114: You say that "only reflectivity in the range of 35 to 70 dBZ was considered in the Analyses", but all of your analysis considers a single threshold of 55 dBZ, so does this filtering really matter? Or are you saying that reflectivities below 35 dBZ or above 70 dBZ were set as missing values?
#We rephrased these sentences for "To avoid this problem, reflectivities below 35 dBZ or above 70 dBZ were set as missing values" (L211-212). The 35 dBZ threshold is used to define and to detect intense precipitation areas by the tracking algorithm. Details about this tracking algorithm and the thresholds used are provided in a new paragraph (now L236-243).

L114-116: This explanation is a little confusing. Looking back at Puskeiler's paper I see that reflectivities have to be >45 dBZ and 5 dBZ or more above the values at the neighbouring grid points to be filtered using Eq. 2. Please rephrase to make this clearer. Also the method doesn't really use a range of 2 km; rather it considers the 8 neighbouring grid points.
#We rephrased this sentence and switch the 2 km range with the 8 neighboring grid points (L213-214). Note that for the Puskeiler et al. (2016) study, the authors applied slightly different methods since the focus there was on 3D reflectivity.

L118: What do you define as "a high reflectivity value"?
#We added an explanation in L216-217. This includes the reflectivity values of the 8 neighboring grid points.

L119-120: I don't understand what you mean when you say "Reflectivity values near neighboring countries were evaluated and calibrate [sic] with radar stations close to the

border." Please elaborate.
#We changed this sentence and added it in L182-184.

L123-125: I've personally never heard of lightning causing spurious radar signatures. If this is a real thing, surely it would represent an argument *against* using lightning data to filter out such signatures?
#We removed "lightning" from the sentence and provided another echo type (L220).

L125-128: While hailstorms typically do produce lightning, I am not aware of any work that shows that this lightning is always cloud-to-ground, which is the only type that you consider in your analysis. As such it is possible that you may have inadvertently filtered out hailstorms that produced only intracloud lightning. This should be noted as a caveat of the method described here.
#We added a sentence explaining why we avoid intra-cloud and cloud-to-cloud lightning (L195-197) and we agree that some hailstorms may have been inadvertently filter out in our analysis.

L140-141: Is tracking only applied to reflectivity areas of ≥55 dBZ? This is a very high threshold for defining convective cells and is likely to lead to much shorter tracks than one would achieve using a more typical threshold such as 35 dBZ. It will also lead to an unrepresentative estimate of the location of convective initiation (Fig. 9), since developing cells may travel some distance before they achieve reflectivities as high as 55 dBZ. In my view, a better approach would be to identify and track cells using a lower threshold, but then only retain those that reach a reflectivity of at least 55 dBZ. This would also allow you to perform a comparative analysis of hailstorms and non-hailstorms. Perhaps this is outside of the scope of the present study, but it would certainly be a nice avenue for future work. At the very least you should note the caveats of using such a high reflectivity threshold for cell identification and tracking.
#We added a short paragraph (L236-240) with descriptions about the tracking algorithm techniques and thresholds used. Convective cells were detected with a 35 dBZ threshold but only grid points overpassing 55 dBZ were suggested to be more able to represent hail and were selected for our study.

L145-148: Looking at Fig. 3a from Puskeiler et al. (2016), the difference in HSS between reflectivity thresholds of 55 and 56 dBZ is very small (both are around 0.6). You should note the corresponding values of POD and FAR: 0.7 and 0.4, respectively. While these values demonstrate reasonable skill, they also indicate that 30 \% of observed hail events are missed while 40 \% of those predicted are false alarms. This provides some idea of the uncertainty in your climatology.
We added a statement about the skill and uncertainty of our climatology in the new manuscript version in L247-252 considering the results of Puskeiler et al. (2016).

L149-159: More details are needed concerning the tracking methodology. For example, what are the intensity and size criteria that are used to match cells between scans? How is a

significantly different cell area defined for the purpose of identifying merges and splits? It might help to add a figure illustrating the process schematically.
#In the revised manuscript we added a detailed description of the tracking algorithm including explanations about thresholds used and how the algorithm tracks convective cells in space and time. This description is now in L253-268.

L165: How is the horizontal wind field estimated? Also, I would describe it as a field of motion vectors, since storms do not move with the wind at any particular level.
We added further details and equations about the computation of the horizontal wind field (L-276-287) and we described it as a field of motion vectors (Equation 2).

L171: You say that ESWD reports were located close to the centre of the storm tracks "in most cases. What percentage of reports were not covered by the tracks? Can you comment on possible reasons (e.g. reflectivity <55 dBZ, erroneous report location/day)?
We added a short explanation in the reviewed manuscript about the percentage of ESWD reports without having a track by following the results of Kunz et al. 2020 who focused on this question and used the same database as in this study (L288-291). We also provide some explanations about possible reasons for ESWD reports not covered by tracks (now L292-294).

L180-182: It is good to reiterate that the 55 dBZ reflectivity threshold doesn't guarantee that hail occurred (and similarly, the absence of such high reflectivities doesn't guarantee that hail didn't occur). At this point you could refer back to section 3.3 where the results of Puskeiler et al. (2016) were discussed.
#We reiterated the fact that the 55 dBZ threshold doesn't guarantee hail on the ground and vice-versa (now line 305 to 307).

L191-194: If the mistral is cold and dry, is it really relevant to hailstorm formation?
#We deleted these sentences.

L263: Hail frequencies are also lower over the high terrain of the Alps and Pyrenees, which is consistent with the results of Nisi et al. (2016, 2018).
#We added these literature suggestion in lines 303-304.

L275: Does the average include only pixels within the area covered by radar? If not, this is how it should be done, otherwise you will artificially lower the average. You also shouldn't include points over the ocean, since these have been masked out in the map plots.
#Yes, the average includes only pixels within the area covered by radar. An ocean mask was also applied on each single radar mosaic so that the data on ocean are filtered out of the analysis.

L299-300: I wouldn't say this result is particularly surprising. Large hail damage simply requires a few storms passing over densely populated areas, whereas Fig. 5 is considering

the average number of hailstorms over a very large area.
We deleted this sentence.

L309: For simplicity, I would make all of the subdomains exactly the same shape and size. It looks like you would only need to modify boxes 11 and 13 for this to be the case. I would also suggest using a consistent 3-letter identifier for all regions, rather than numbers. These could be listed in a key/legend in Fig. 3 or in a separate table. The following would be my suggestions for the identifiers: 1 = NWG (North West Germany), 2 = NEG (North-East Germany), 3 = BEL (Belgium), 4 = WCG (West-Central Germany), 5 = ECG (East-Central Germany), 6 = NWF (North-West France), 7 = IDF (Île-de-France), 8 = LUX (Luxembourg), 9 = BAV (Bavaria), 10 = WCF (West-Central France), 11 = MAS (Massive Central), 12 = SWF (South-West France), 13 = MED (Mediterannean).
We followed this suggestion and changed the sizes of boxes 11 and 13. We also changed the box names by adding the acronyms suggestions of the reviewer (Figure 3) and applied a Lambert Conic projection on the map.

L316: It doesn't make sense to simply accumulate the number of hail days over all grid points in each subdomain. For one thing, some of the subdomains contain large areas that are over the sea and/or outside of radar coverage, which will give them a lower number than subdomains that are entirely over land and within radar coverage. It is also very difficult to interpret what these numbers mean. Instead, you should calculate the average number of hail days over all points with data (i.e. excluding those over the ocean and outside of radar coverage). This approach will give a much fairer comparison between the different regions. It's a good idea to use a moving average; however, from Fig. 3 it appears that you consider the preceding 10 days for this average. Instead, I would recommend using a 15-day moving average centred on the day in question (i.e. ±7 days).
#We computed the average number of hail days. The changes are described in lines 451-485 and appear on figure 7. After having tested different moving averages (5, 7, 10, 15 and 20 days), a 10-day moving average was the best representation of the temporal hail distribution of each subdomain.

L363: Again, you should consider the average number of hail days for each hour, not the total number of days over the domain. Also, why only consider the first time that a reflectivity of 55 dBZ is detected? Surely you should consider all times with 55 dBZ or higher in order to properly capture the diurnal cycle of hail (not just its initiation)?
#We computed the average number of hail days for each hour (new Figure 8) instead of counting the total number of days over the domain. We kept the first time when reflectivity overpassed 55 dBZ as the motivation was actually to investigate where the first hail signals appear (e.g. near topography?).

L397-409: The problem with this analysis is that it assumes that the first detection of reflectivity ≥55 dBZ corresponds to the initiation of convection. In fact, developing convection may travel some distance before it reaches such an intensity, particularly in the presence of strong background flow (which would be expected in high-shear environments that favour

severe storms). This is one reason why it would be advantageous to use a lower reflectivity threshold for identifying and tracking convective cells. At the very least, this caveat needs to be mentioned.
#Few thresholds were in fact used for the detection of convective cells and hailstorms. We kindly refer the reviewer to Section 3.3.

L418: You can probably just say lengths "between 10 and 20 km". Using 10.1 km as the lower bound implicitly excludes tracks with a length >10 km but <10.1 km. Alternatively, if you want to be more precise, you could define a variable L to represent track length and then use "10 < L ≤ 20 km" to represent this particular bin. Either way, the same change should be applied on L420.
#We used the sentence suggested by the reviewer: "a length L between 10 and 20 km" (L540).

L423-426: How did these studies define hail cells? If they used a lower reflectivity threshold, they are likely to get longer hail tracks because they will be including storms at earlier and later stages of their life cycles and are also less likely to break up tracks where the reflectivity temporarily drops below 55 dBZ.
#They used 3D (not 2D) radar data and applied a different algorithm (lines 549-551) to identify hail cells.

L427-428: While the results for hail track duration may be similar to those for track length, it would still be nice to include the results in Fig. 10. You could also (or alternatively) combine length and duration to compute storm motion estimates for each cell and examine the distribution of this.
#We added Figure 11 showing the mean duration and described the results in L552-554.

L429-432: It would make more sense to compute the track width as the average diameter or the cell (computed over its lifetime) in the direction perpendicular to its movement, since this will actually correspond to the width of the underlying hail swath (under the assumption that hail falls where reflectivity ≥55 dBZ). If you make this change, I would strongly encourage you to include the results in Fig. 10.
#Only the track width maximum was stored by the algorithm.

L433-436: Again, rather than considering cells at a particular time, why not use the whole swath? For orientation, you could compute it simply as the angle between the first and last points in the trajectory (similar to how you define track length). Alternatively, you could apply a line of best fit to the set of points defining the trajectory. I would recommend a Theil-Sen fit for this purpose, as it is less sensitive to outliers for small sample sizes, compared to a linear least squares fit. Also, you should note that the angle is defined as the direction from which the storm is coming and is measured clockwise from north.
#We described how the angle is defined in L559-561. The methods described by the reviewer fit for straight (e.g. undeviated) swaths only. In case of a change of storm direction (which was for example the case in July 2013 in Southwest Germany after a cell splitting) the swath is bending

and shows multiple orientations. Thus, the orientation of the swath on a given time is more precise than a computation of the orientation between the starting and ending swath point.

L467-468: The key issue with the lack of 3D radar data is the inability to use more sophisticated proxies such as those based on echo-top height (e.g. POH) or vertical integrals of reflectivity (e.g. MESH), which generally show higher skill in hail prediction (e.g. Skripniková and Řezáčová2015; Kunz and Kugel 2015; Puskeiler et al. 2016).
#We added a comment in L592-594 about the key issue with the lack of 3D radar data and we have added the literature suggested by the reviewer.

Figure 3: I would recommend presenting these results as annual hail frequencies rather than counts of the total number of hail days. This will make it easier to compare your results with climatologies for different periods (including the maps for 2006 and 2010 in Fig. 6) and in other parts of the world (e.g. Cintineo et al. 2012; Warren et al. 2020). Also, you should mask out those grid points that fall outside of radar coverage, as shown in Fig. 2.
#We followed this suggestion and presented the results as annual hail frequencies rather than the total number of hail days (new Figure 3).

Figure 4: For the zoomed in view of the Massif Central region, it looks like you've just cut out and blown up a section of the fairly coarse-resolution image on the right. As such it's very difficult to make out the details in both the orography and the hail frequency contours. I don't think you need the map of the full study domain as this is already shown in Fig. 1. Instead, I would make this a multi-panel figure, showing zoomed-in views (at an appropriately high resolution) for several of the hail hotspots visible in Fig. 3 and discussed in section 4.1.
#We deleted the coarse resolution zoomed-in-view of the Massif Central and replaced it by a high-resolution Global relief map overlaid with hail frequency contours and wind flow during hail days (new Figure 4). The results were described in Section 4.1.

Figure 5: Please present these data as the actual number of hail days for each year rather than the difference from the mean (which can easily be inferred).
#We presented the data as actual number of hail days for each year in the new Figure 5.

Figure 7: As noted above, rather than the total number of hail days in each subdomain, you should plot the mean number of hail days (excluding points that are over the sea or outside radar coverage). The same change should be applied to Fig. 8.
#We changed the total number of hail days for the mean number of hail days for Figures 7 and 8.

Figure 9: It would be nice to show these plots for other hours, rather than just 02 and 18 LT. For example, you could group the data into 3h blocks (00-03, 03-06, 06-09, 09-12, 12-15, 15-18, 18-21, and 21-00 LT) and present the results as an 8 panel figure.
#We added a 8-panel figure following this great idea (now Figure 9).

Technical Corrections

I am not sure what the standard is for this journal, but in English (both American and British), a period is used as the decimal separator and a comma (or sometimes a thin space) is used to break up numbers of ten thousand or higher. For example, twelve-thousand three-hundred and forty-five point six would be written as 12,345.6.
L10-11: Change "spatially most extended" to simply "longest".
L12: Change "implied" to "produced" or "were associated with".
L12-13: Change "2 Billions Euros" to "€2 billion".
L20: This is not the correct use of "respectively" - it should only be used when describing two or more items that refer back to a previous statement. For example, "in northern Germany and southern France, hail occurs most frequently in August and June, respectively". The same comment applies to L96 and L269.
L23: Change "major part" to "majority".
L31: Puskeiler et al. (2016) consider the years 2005-2011, not 2004-2014.
L34: Change "criterions" to "criteria". Also "echo top" should be two words.
L46: Change "allows" to "allow".
L47: "sea" shouldn't be capitalized.
L213: Change "weaker" to "lower".
L229: Get rid of "recently".
L317: I think you meant to put "(Figure 7)" at the start of this line.
L386: The definition of overshooting tops should be given when they are introduced on L37.
L394: This doesn't need to be a new paragraph.
L421: Get rid of "including squall lines". Also, it should be "MCSs".
L446: "...from French and German national radar composites..."
L448: Duplication of "Mason".
L557: Get rid of "to" before "orography".
L466-467: Change "allows obtaining hail proxies" to "provides a proxy for hail occurrence".
Figure 1: Please use different line thicknesses, styles or colors to distinguish between country and state/distinct borders. The same applies to Fig. 3, 4, and 6.
Figure 6: The colour bar is incorrectly labelled. The number of hail days in a single year will always be an integer, so you don't need the range or the decimal place (i.e. the labels should just be 1, 2, 3, ⋯, 12).
Figure 10: The x axes of these plots are incorrectly labelled. Each bin corresponds to a range of values, so the tick labels should be located under the ticks to illustrate this. So, for example, for panel (a) the ticks should be labelled 0, 10, 20, ⋯, 310.

#All the technical corrections listed above have been inserted in the new paper version.

References

Cintineo, J.L., Smith, T.M., Lakshmanan, V., Brooks, H.E. and Ortega, K.L. (2012) An objective high-resolution hail climatology of the contiguous United States. *Weather and Forecasting* , **27** , 1235‑1248.
Louf, V., Protat, A., Warren, R.A., Collis, S.M., Wolff, D.B, Raunyiar, S., Jakob, C. and Petersen, W.A. (2019) An Integrated Approach to Weather Radar Calibration and Monitoring Using Ground Clutter and Satellite Comparisons. *Journal of Atmospheric and Oceanic Technology* , **36** , 17‑39.
Skripniková, K. and Řezáčová, D. (2014) Radar-based hail detection. *Atmospheric Research* , **144** , 175‑185.
Soderholm, J., McGowan, H., Richter, H., Walsh, K., Weckwerth, T. and Coleman, M. (2017) An 18-year climatology of hailstorm trends and related drivers across southeast Queensland, Australia. *Quarterly Journal of the Royal Meteorological Society* , **143** , 1123‑1135.

#We thank the reviewer for providing the literature and added it to the new manuscript.

Answers for Anonymous Referee #2

The paper "Radar-based assessment of hail frequency in Europe" is targeted on climatology of severe convection storms (SCS) based on 10 years of radar data covering a large European region. The topic is very important and suitable for NHESS. The analysis covers a relatively large number of years (considering typical radar records) and geographic domain.
#We thank again the reviewer for spending time on reading the paper and for the relevant suggestions. In the revised version, we addressed comments for every major and minor issues in green color.

My main concern is if we are really sure these are hail cases. The paper, is it is now, is not clear about this. The text some times refer the data set as SCS and sometimes as hail cases.
On one hand, it seems some validation has been done: "Tests with long-living SCS tracks were compared with hail reports archived by the European Severe Weather Database (ESWD) operated by the European Severe Storms Laboratory (Dotzek et al., 2009) along the reconstructed storm trajectories to assess the reliability of CCTA2D (not shown). In most cases, the ESWD reports were located close to the center of SCS tracks." (Lines 169-172). But, just next to it, at the beginning of the results section, there is a "disclaimer": "Note that this climatology represents the spatial distribution of convective cells with high reflectivity, but not directly of hail. The term hail days used in the following refers to the exceedance of reflectivity, but not to confirmed hail observations" (Lines 180-182). I understand the first case refers to tracks while the second to the spatial distribution, but I think it would be better to clarify in a targeted section whether or not there is any validation that the analyzed storms are indeed hail events. Also, through out the text try to be more consistent in the use of SCS vs. hail events according to the level of assurance of the nature of these events.
Furthermore, validation seems quite crucial here, as without it, the data set may not represent hail events. So I encourage the authors to present the validation done against the hail reports from ESWD and if possible to extend it.
#We reiterate that an identification of hail within the SCS tracks and especially a separation between hail and heavy rainfalls is not possible giving the lack of comprehensive hail observations and the use of a proxy. Concerning the validation of tracks with ESWD reports, we mentioned in the new manuscript the main results established recently by Kunz et al. (2020) who worked with the same dataset as in this study. By using ESWD reports in the vicinity of SCS tracks, the authors could separate the SCS-tracks into two categories: Hailstorms (having a ESWD report near a track) and other Convective storms (tracks without nearby ESWD report) but that may also include few hailstorms (L288-292). We finished by listing the different reasons why a track could not be associated with a hail report (L292-294).

Other comments:
It would be good to provide a short background on hail formation, under what meteorological conditions we should expect hail events. This would help in understanding the interpretation of the presented results.

#We dedicated a paragraph (L18-36) on hail formation, describing the diverse processes and mechanisms leading to hail formation in convective clouds and added few assumptions about the ambient conditions favoring hailstorms in Europe.

The data set includes radar data from two countries which goes some different processing procedures. To be sure this does not add any bias in results – is there any overlap region where analysis from both data sources can be compared?
#We added a comment on that in L182-184, where we mention that the Rhine Valley is an overlapped region between France and Germany. During hailstorms crossing both France and Germany, we compared reflectivity values measured from both German and French radars. Only small differences appeared between the radar reflectivity datasets. These differences are corrected with our tracking algorithm using an advection correction along the wind field, and it induces a smoothing of the reflectivity values.

Lightening filter: "If high reflectivity during a day occurs without lightning, the values at the affected grid points are set to zero." (Line 127-128): why only during day? Are you sure this filter is not too aggressive? Can you provide any information on percent of hail storms that are not associate with lightening? if I understand correctly these storms will be filtered out from the analysis and it is important to verify their fraction is not substantial.
#We clarified in line 224 that the filter runs for day and nighttime (day in the sentence is meant as 24-hour period).

Split and merge: the authors write that "Special attention is given to cell splitting and merging" (Line 154). Why is that? I did not find in the results any consideration of the splits and merges that were detected.
#We added an explanation about storm splitting and merging in lines 258-268 and mentioned that the results in this study include both of them.

Line 277: "As shown in Figure 5 the annual variability is very high and without any trend" – for 10 years of data I would not consider a trend for 10 years of data.
#We deleted "without any trend" and replaced the sentence with : "Averaged over the entire investigation area, the annual number of hail days is between 72 (2010) and 103 (2006) with a mean of 86 (Figure 5)."

Line 283-285: "large-scale lifting (e.g., related to differential vorticity advection) could have led to an increase in convective available potential energy (CAPE) and a low convective inhibition (CIN). The combination of high moisture in the boundary layer, low CIN, high CAPE and lifting mechanisms may give rise to a substantial increase in SCS." It is not clear if this is an assumption or analysis. Why not to check reanalysis data for CAPE, CIN, air moisture anomalies? without it, I think this sentence is too speculative.
#We deleted this speculative statement.

General comment: the authors provide a very detailed description of the pattern shown in the figures. In my opinion this is too lengthy and could be shorten. I leave this however for the author decision.

#We did try to shorten some pattern descriptions and keep the essential parts only. However the area we investigate is large and the authors found it interesting to describe the hail variability towards Europe.

List of all relevant changes made in the new manuscript

1. In subsections 2.1.1 and 2.1.2: We added a description of the processing stages performed to produce the French and German national radar composites. This summarizes long technical reports provided by the French and the German National Weather Services.

2. A relevant contribution to the new paper version is the investigation of the role of topography on hail formation. For this purpose, we computed the flow (wind speed and velocity) at 10m during hail days using ERA-5 reanalysis for all subdomains described in this study and computed each time the Froude Number to assess the flow deviation in the vicinity of the topography. For each subdomain, the flow, as well as hail hot spots contours were added on a high-resolution relief map (ETOPO-1). In the new manuscript version, we show the results for the subdomain including the Massif Central only (in Figure 4) in order to avoid a too lengthy manuscript. The description of the wind flow in the Massif Central region is available in L-316-146.

3. Figures: We changed the design of Figures 5, 7, 8, 10, 11 and 12 in the new paper version. Additionally, Figures 7 and 8 present now the average number of hail days rather than the total number of hail days. In the new manuscript, we also added a 8-panel Figure (Figure 9) of the locations of the first convective signatures detected by the tracking algorithm. Furthermore, in the new revised manuscript, all maps were projected on a Lambert Conformal Conic Projection rather than the previous Pseudo Plate Carree projection.

Radar-based assessment of hail frequency in Europe

Elody Fluck[1,*], Michael Kunz[1,2], Peter Geissbuehler[3], and Stefan P. Ritz[3]

[1]Institute of Meteorology and Climate Research (IMK), Karlsruhe Institute of Technology (KIT), Karlsruhe, Germany
[2]Center for Disaster Management and Risk Reduction Technology (CEDIM), Karlsruhe, Germany
[3]RenaissanceRe Europe AG, Zurich, Switzerland
[*]now at: Department of Earth and Planetary Sciences, Weizmann Institute of Science, Rehovot, Israel

Correspondence: Elody Fluck (elody.fluck@weizmann.ac.il)

Abstract.

In this study we present a unique 10-year climatology of severe convective storm tracks for a larger European area covering Germany, France, Belgium, and Luxembourg. For the period 2005-2014, a high-resolution hail potential composite of 1×1 km^2 is produced from two-dimensional reflectivity radar data and lightning data. Individual hailstorm tracks as well as their physical properties, such as radar reflectivity along the tracks, were reconstructed for the entire time period using the Convective Cell Tracking Algorithm (CCTA2D).

A sea-to-continent gradient in the number of hail days is found to be present over the whole domain. In addition, the highest number of severe storms is found on the leeward side of low mountain ranges such as the Massif Central in France or the Swabian Jura in Southwest Germany. A latitude shift in the hail peak month is observed between the northern part of Germany where hail occurs most frequently in August, and southern France where the maximum of hail is two months earlier. The ~~spatially most extended~~ **longest** footprints with high reflectivity values occurred on 9 June 2014 and on 28 July 2013 with lengths reaching up to 500 kilometers. Both events ~~implied~~ **were associated with** hailstones measuring up to 10 cm which caused damage in excess of ~~2 Billions Euros~~ **€2 billion**.

1 Introduction

Severe convective storms (SCS) and related hail constitute a major atmospheric hazard. These events have the potential to cause substantial damage to hail-susceptible objects such as buildings, crops or automobiles, in various parts of Europe, including France, Germany, Austria, and Switzerland (e.g., Dessens, 1986, Puskeiler et al., 2016, Nisi et al., 2016). Prominent examples are the two hailstorms related to the low-pressure system Andreas that occurred on 27/28 July 2013 over central and southern Germany with total economic losses estimated to approximately ~~EUR~~ ~~€~~3.6 billion (SwissRe, 2014, Kunz et al., 2018). **Hail occurs in organized convective storms (Auer, 1972) that is, multicells, supercells or Mesoscale Convective Storms (Markowski and Richardson, 2010), and results from the interaction between diverse processes and mechanisms on different spatio-temporal scales. Several authors have studied environmental conditions favoring hail production (Dessens, 1986, Houze J, 2014, Kunz et al., 2020 among others). In general, a subtile interplay between three main ingredients supports the formation of deep moist convection (Kunz, 2007): 1) Thermal instability represented, for example, by a**

decrease of equivalent potential temperature with height permits an air parcel to rise vertically to a considerable height (Holton, 2004) due to positive buoyancy; 2) A high moisture content in lower atmospheric levels lowers the level of free convection (LFC) in a cloud and increases convective available potential energy (CAPE); and 3) a lifting mechanism to trigger convection such as orographic lifting (Kirshbaum et al., 2018, Barthlott et al., 2016) or lifting associate with synoptic cold-fronts (Kunz et al., 2020). Vertical wind shear is another parameter mainly relevant for the organization form of the storm and, thus, also for its lifetime, and severity. Several authors found that large hail preferably occurs in strongly sheared environments, supporting the formation of supercells (Kunz et al., 2020, Pilorz and Łupikasza, 2020). Aside of the parameters mentioned above, some authors found that an increased frequency of SCS in Europe can be associated with specific large-scale flows or teleconnection patterns (Piper et al., 2019, Mohr and Martius, 2019, Kunz et al., 2020). Several authors found for example a configuration where the East of the Atlantic Basin is dominated by a low pressure area and where France lies under a ridge (Piper et al., 2019, Fluck, 2018). This latter weather pattern favors the advection of moist and warm air on the lower atmospheric levels coming from Iberia and moving towards West Europe. Such a weather setup is termed Spanish Plume by Morris (1986). This feature is related to a trough centered over Western Europe or the Eastern Atlantic and the subsequent southwesterly winds crossing the Mediterranean Sea permits the impinging of moist and warm air masses into Central Europe. Such a configuration may increase the hail potential over western Europe by the creation of low thermal stability, a capping inversion and sometimes an elevated mixed layer (EML).

A major obstacle when investigating hail events and their climatology **~~, respectively,~~** is the lack of accurate and comprehensive observations. This observation deficit is because of the local-scale nature of SCS and the even smaller hailstreaks with a small spatial extent (Changnon, 1977). There are only some high-density, regional-scale ground detection networks using hailpads for recording hail fall in operation, such as in southwestern and central France (Dessens, 1986, Vinet, 2001), parts of Spain (Fraile et al., 1992) or norther Italy (Eccel et al., 2012). The **~~major part~~ majority** of Europe, however, remains uncovered by a hail network leading to a gap in direct hail observations. Therefore, little is known about the local-scale hail probability and related hail risk across Europe.

Numerous authors haved used hail signals derived from conventional weather radars for the identification and analysis of hail because of their high temporal and spatial resolutions. For example, Nisi et al. (2016) and Nisi et al. (2018) established a hail climatology for Switzerland from 2002 to 2014 based on both Probability of Hail (POH) and Maximum Expected Severe Hail Size (MESHS) estimated from volumetric (3D) radar data. Puskeiler et al. (2016) used 3D radar reflectivity together with modelled melting layer, lightning data and the cell-tracking algorithm TRACE3D (Handwerker, 2002) to reconstruct hailstreaks and, from that, to estimate the hail frequency across Germany between **~~2004 and 2014~~ 2005 and 2011**. Combining 3D radar reflectivity and insurance loss data for buildings, Kunz and Puskeiler (2010) found the highest hail frequency in Southwest Germany to be located downstream of the Black Forest mountains. This hot spot was also confirmed by Kunz and Kugel (2015) using five different hail **~~criterions~~ criteria** based on 2D and 3D radar reflectivities and different heights (melting layer, **~~echotop~~ echo top**). Lukach et al. (2017) computed a hail frequency map for Belgium from 2003 to 2012 using 3D radar data. **Outside of Europe, Cintineo et al. (2012) produced a high-resolution hail frequency map for the**

USA from 2007 to 2010 using MESH (Maximum Expected Size of Hail) product. The authors found a high hail frequency during March to September (with June as a maximum) in the Great Plains. More precisely, the highest hail frequency is mainly centered over the southern part of the Great Plains from March until May, while from July to September, hail is more frequent in the central and northern plains. The MESH product was also used in the studies conducted by Warren et al. (2020) in Australia where the authors used daily grids of merged radar data including MESH at a 1 km resolution from 2009 until 2017. A pronounced peak of hail appeared during (souther-hemisphere) summertime, in December on the coastal slopes of the Great Dividing Range. In Czechia, Skripniková and Řezáčová (2014) used the Waldvogel criterion on single-polarisation radar data to retrieve hail signals for the period 2002 until 2011. The authors found that hail occurred mostly during May, June and July during the afternoon throughout the country. Despite the use of improved radar-based techniques, most of the studies cited above were restricted to smaller regions or a single country. While some authors have estimated hail frequency from other sources such as Overshooting Tops **~~OT~~ ,"a domelike protusion above the cumulonimubs anvil, representing the intrusion of an updraft through its equilibirum level" according to the American Meteorological Society (Glickman and Walter, 2000), ~~from detections~~** in satellite imagery (Punge et al., 2014), model data (Mohr et al., 2015b, a; Rädler et al., 2018) or a combination thereof (Punge et al., 2017),**~~these methods are not as straight forward as those based on radar reflectivity~~ the link between the observed quantities and hail occurrence at the surface is less reliable than using radar measurements**. Numerical models, such as weather forecast or regional climate models (RCM), on the other hand, are not able to reliably reproduce hail due to a high degree of uncertainty in the initial conditions, a lack of knowledge in cloud microphysics, and the high computer costs when running a two- or three-moments microphysics scheme.

The objective of our study is to analyze the spatiotemporal variability of hail signals over a 10-year period (2005 to 2014) covering the four European countries of France, Germany, Belgium and Luxembourg. Hail signals were estimated from 2D radar reflectivity available for each country, which permits a homogeneous hail analysis. The results help to identify regions frequently affected by hail and **~~allows~~ allow** us to relate hail frequency to topographic features such as terrain height or the proximity to the **~~Sea~~ sea**. A thorough study of hail events gives further insights into the relation between orography and deep moist convection. Improved understanding of these mechanisms and processes is crucial to improve the nowcasting and forecasting skill of hail storms. Finally, as hail constitutes a considerable risk for the insurance industry, improved knowledge about hail frequency**~~, intensity,~~** and hailstorm characteristics will help to better understand the related risks.

The paper is structured as follows: Section 2 gives an overview of the remote-sensing and reanalysis datasets used for this study. Section 3, describes the combination of radar data with lightning data and the application of the tracking algorithm. The remote-sensing output is then used to generate European composites at 5-minute time steps. Section 4 assesses the hail variability between 2005 to 2014 in relation to the distance to the sea and the presence of orography near hailstorms. **This section also presents results on seasonal and diurnal variations in hail frequency and provides some characteristics of the hail cells.** Concluding remarks follow in Section 5.

2 Datasets

2.1 Remote-sensing data

In this paper, we present a hail climatology retrieved from radar reflectivity datasets available from the first phase of the project HAMLET (Hail Model for Europe by Tokio Millennium) that lasted from 2013 until mid-2017. 2D radar reflectivity for the summer half-years (April to September) from 2005 to 2014 for Germany, France, Belgium, and Luxembourg are considered (Figure 1). **The French national radar composites were available until 2014 only, due to the installation of five new X-band radars in the Alpine region in 2014 (See Section 2.1.1) that requested some computation adjustment into the national radar composite. The French national radar composites from 2014 up to nowadays including the X-band radars in the Alpine region installed in 2014 were available only later.** The radar products used in this study are composites of the Maximum Constant Altitude Plan Position Indicator (MaxCAPPI), where the composite is a merger of the data from all local radar stations in a single image at time steps of five minutes. 2D radar data are used here because of the large domain and their long-term availability.

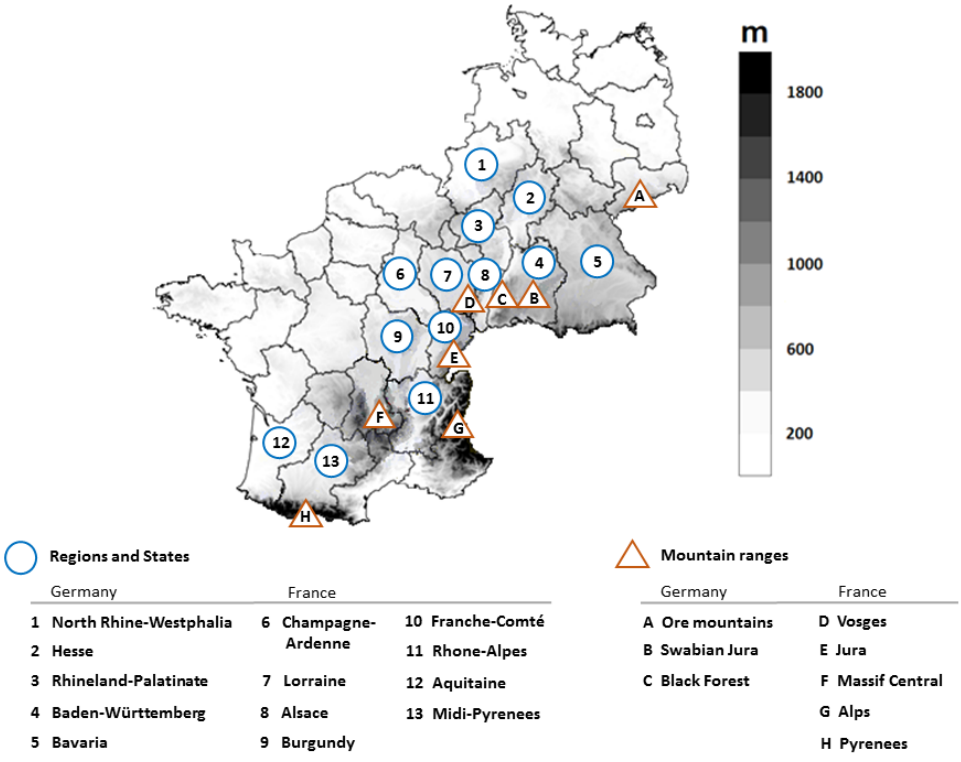

Figure 1. European regions and mountain ranges mentioned in this study.

2.1.1 French radar data

The French radar network operated by Météo-France and the derived radar products evolved constantly through times, mainly via national projects. A brief overview of the French radar network is given hereafter. The project Panthère launched in 2002 (Parent du Châtelet et al., 2005) permitted to add 6 new radars to the previous 19 radars constituting the French radar network in 2001. During this operation, some of the 19 radars were replaced by dual polarization radars (Tabary et al., 2006, Bousquet et al., 2008). In 2005, 24 radars were in operation including 19 C- band radars and five S- band radars (both with a radius of up to 120 km). ~~**The French radar network operated by Météo-France included 29 radar stations in 2015 with 19 C-band radars, five S-band radars (both with a radius of up to 120 km).**~~

Two years later, in 2007, the radar stations of Toulouse in southwestern France and Trappes (near Paris) were renewed in the course of the same project Panthère (Tabary, 2007) but this replacement did not affect the radar national composite. During the period from 2007 to 2011, the radars of Plabennec located in northwestern France, Abbeville in northern France, Nimes in southern France and Grèzes in the southern part of central France were replaced as well with dual polarization radars. In 2014, five X-band radars with an average coverage radius of 50 km **were added to the French national radar composite** (Figure 2) **via a project named RHyTMME (Risques Hydrométéorologiques en Territoires de Montagnes et Mediterranéens) described in the study of Beck and Bousquet (2013) with the objective to improve the hydrological risks management in the southern Alps region (Champeaux et al., 2011)**. As the data from the X-band radars were only recently implemented into the French national composite (Yu et al., 2018), only S- and C-band radars were considered in this study.

Concerning the scanning strategy, four to six scans are performed every 15 minutes at elevation angles ranging from 0.4° up to 15° (Figueras i Ventura and Tabary, 2013). Only the lower elevation angles below 2.7° are scanned every 5 minutes. The radar stations of Avesnois (located in northern France) and Réhicourt-la-petite in Lorraine (mentioned as region number 7 in Figure 1) cover a large part of eastern France, and permit to integrate Luxembourg completely, as well as a significant part of Belgium, into the French national composite. The spatial resolution of the composite is 1×1 km^2 with a size of 1536 × 1536 grid points for each image referred to a plane Cartesian coordinate system (Tabary et al., 2006). **Radar data from all stations are pre-processed via an algorithm (Tabary, 2007) named Castor2 (Figueras i Ventura et al., 2012), which corrects for several errors, such as antenna positioning errors, and quantifies horizontal reflectivity Z_h (and differential reflectivity Z_{dr} or correlation coefficient ρ_{hv} for dual-polarized radars) in polar coordinates (Tabary, 2007). During the pre-processing stage, each radar pixel receives a weighted quality index (QI) ranging from 0 to 1 (Tabary, 2007), updated throughout the whole pre-processing chain. The first pre-processing step is to eliminate ground clutter, i.e., fixed echoes at the surface, using Doppler velocity (Tabary et al., 2013). Then an orographic mask is applied at each elevation angle in order to assess the beam occultation rate. After that, an "anthropogenic" mask, including buildings, trees, or other fixed objects in the vicinity of the radar is computed with the help of long-term accumulated radar products. These masks allow to remove radar pixels with artificially high reflectivity at each elevation angle. Beam widening, i.e., the increase of the radar volume with distance to the radar, is taken into account (Tabary et al., 2013)**

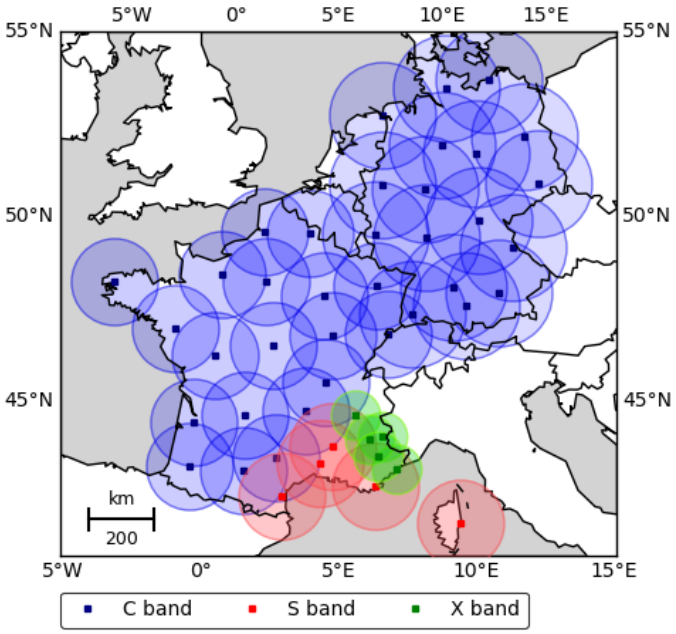

Figure 2. Locations (squares) and coverage of the radar stations (circles) in 2014 used in this study. See text for further explanations.

using vertical reflectivity profiles. Attenuation by oxygen is corrected depending on the wavelength, the elevation, and the distance to the radar (Doviak and Zrnić, 2006). For example, a correction of 1.79 dBZ at 100 km away from the radar site is applied to C- band radars for an elevation angle of 0.4° (Tabary et al., 2013). One of the last pre-processing step is the correction of the bright band with the help of vertical reflectivity profiles. After performing all the steps described above, individual plan position indicators (PPIs) are combined to 2D composites produced every 5 minutes available for each radar station to estimate the intensity of rainfall by converting the reflectivity data into rain rate using the $Z - R$ relation according to a Marshall-Palmer distribution (Tabary et al., 2013). During this step each pixel is assigned a QI ranging from 100% (excellent) to 0% (poor) resulting from the previous weighted QIs (Champeaux et al., 2011). A pixel with a QI of less than 80% is automatically removed from the rainfall product. The final step of the pre-processing is the Quantitative Precipitation Estimation (QPE) calibration with rain gauge data by using the large rainfall network operated by Météo-France including approximately 900 automatic stations (Champeaux et al., 2011). A weighted calibration of the QPE is performed with real-time, hourly rain gauge data. After performing the pre-processing chain, all individual radar products are combined into a national mosaic (Augros et al., 2013). For areas with overlapping radar coverage, weighted reflectivity data are computed depending on the distance to the nearest radar (Tabary et al., 2013). At the boarders of France, radar data from other national weather services are integrated into the French national mosaic.

~~**Radar data quality has been checked several times for the French radar network, like Gourley et al. (2006),**~~

~~who proceeded to a quality check of C-band radars. Furthermore, a radar correction algorithm including beam-blocking correction and ground-clutter identification was applied on the French reflectivity mosaic (Tabary, 2007).~~

Reflectivity values **from the French radar mosaic used in this study** were coded in a table and stored in GeoTIFF format, i.e., georeferenced TIFF images. The resolution is 2×2 km^2 from ~~1999~~ **2004** until mid-June 2009, and a finer resolution of 1×1 km^2 is available from ~~the end of June~~ **mid-June** 2009 to 2014. For data homogenization, each of the 2×2 km^2 composite was interpolated linearly from 2004 to June 2009 to the finer grid of 1×1 km^2.

2.1.2 German radar data

The German radar composites for the period from 2005 to 2014 are provided by the German Weather Service (DWD), which operated a network of 17 C- band radar systems in ~~2016~~ **2014**. **During the investigated period, a new radar in Memmingen, southern Germany, was added to the network in 2012 (Puskeiler, 2013).** As the horizontal range detection for each radar is 180 km and a maximum distance of 200 km separates the radar stations, an extensive overlap of the detection areas permits almost a complete coverage of the German territory. Only some peripheral regions remain as gaps in the composite, for example, in the far North near the Danish border or in southeastern Bavaria (Figure 2). In the complex terrain of southern Germany, weather radars are preferably located on hills and mountains to minimize beam shielding by orography. **Concerning the scanning strategy, the lowest elevation angles between 0.5° and 1.8° (Bartels et al., 2004) at that time were scanned every 5 minutes, whereas a complete volume scan took 15 minutes. The maximum reflectivity values of the lowest elevations are used for the national 2D reflectivity composite. The steps of the pre-processing are similar to those of Météo-France, and include among others: An elimination of clutter pixels using a clutter filter, orographic shading correction using an elevation model, transformation of reflectivity Z to rain rate R. After the pre-processing, the local radar data are merged into the German national composite. For areas with overlapping radar coverage the maximum reflectivity value from all radar scans is used in the composites, while for the neighboring regions of foreign countries, a weighted adjustment is performed between radar products from other national weather services and the German rain-gauge dataset (Kreklow et al., 2020). The quality of German radar data has improved over the last decade with continuous algorithm corrections and adjustments (Kreklow et al., 2020) used for RADOLAN (Radar-Online-Aneichung, which means Radar-Online Adjustment) and can be assessed by a quality flag provided for each pixel on the reflectivity product.** The spatio-temporal resolution as well as the time period available for the German radar data is the same as the French, namely 1×1 km^2 with a 5-minute time step for the composite and available from 2005 until 2014, so that both data sets can be merged. The encryption of each scan of the DWD network entails raw terrain-following near ground reflectivity (CAPPI) values (named RX product) in so-called RVP6 units. ~~**The conversion from RVP6 to dBZ is as follows:** $dBZ = (\frac{RVP6}{2} - 32.5)$ **The accuracy of the RVP-6 units is 0.5 dBZ in a range from 0 to 255.This corresponds to a reflectivity from -32.5 to 95 dBZ.**~~ The advantages of this data are the high temporal and spatial resolution which enables us to properly identify footprints of SCS. RX data are projected on a Cartesian grid so that each grid box is equidistant at 1.0 km. In the end, the German radar composite has a size of 900×900 km^2 covering the whole of Germany.

2.1.3 Uniform Pan-European Grid

It is important to note some limitations in both the German and French national composites. Long-term QPE maps for the French national composite reveal some regions with low data accuracy. This is mainly the case for the central and eastern part of the Pyrenees mountains and the entire Alpine region (Tabary et al., 2013). In the other parts of France, the QI is mostly higher than 90% with especially high QI close to the radar site (Tabary et al., 2013). Radar data failure, for example during radar calibration, or radar replacement, were estimated by Puskeiler et al. (2016) to be approximately 4.5 ± 3.9% on average (mean ± standard deviation for the German national composite). Furthermore, the combination of the German and French national composites, each calibrated and pre-processed in different ways, may lead to inhomogeinities in relative hail frequency in some regions. Based on manual investigation of several cases with severe hailstorms in the border region between Germany and France, it was found that the signal of the French mosaic is between 0.5 and 1 dBZ lower compared to that obtained from the DWD composite (Schmidberger 2020, personal communication). This uncertainty is acceptable when projecting the two national composites onto a uniform Pan-European Grid. Radar reflectivity data and thus radar-derived hail signals ~~, respectively,~~ were projected on the same uniform European grid (not shown) with a resolution identical to that of the national radar network (1×1 km^2). ~~The grid uses the standard coordinate system and the standard spheroidal reference surface defined by the World Geodetic System elaborated in 1984 (WGS84)~~ **We used the geographic coordinate system WGS84 for the Pan-European Grid and a Lambert Conformal Conic Projection, as recommended by Gregg and Tannehill (1937) and Varga (1990).** In the center at about 47°N and 6°E, the meridional grid spacing is equal to the zonal direction to minimize the grid distortion.

2.1.4 Lightning data

To remove artificial clutter still present in the data, we additionally implemented a filter based on lightning data, which was already used by Puskeiler et al. (2016). Here we used only cloud-to-ground (CG) lightning (strokes) from the low-frequency lightning detection system BLIDS (BLitz InformationsDienst Siemens), which is part of the EUCLID (EUropean Cooperation for LIghtning Detection) network. The detection efficiency of the system is 96% for strokes with a peak current of at least 2 kA (Schulz et al., 2016). Because the sensors and the algorithm implemented until 2015 had a significantly lower detection efficiency of intra-cloud and cloud-to-cloud lightning according to Pohjola and Mäkelä (2013), these types of lightning were not considered.

2.1.5 ERA5 reanalysis

To assess the mean wind flow during hail days, we used the ERA5 global reanalysis (Hersbach et al., 2020). ERA5 is a new global atmospheric reanalysis recently released by the ECMWF and aims to replace ERA-Interim reanalysis (Dee et al., 2011) whose data extend from 1979 to 2019. For the moment, ERA5 is available from 1979 onwards and will be soon extended to 1950. The ERA5 4D-Var analysis dataset is assimilated by the Integrated Forecasting System (IFS)

and is available on a horizontal resolution of 31km on 137 vertical levels every hour.

3 Methods

3.1 Correction of erroneous signals

Concerning the homogenization of the French and German national composites, several corrections had already been performed by both national meteorological services. Radar reflectivity data still contains noise and systematic errors that have to be eliminated using various approaches. Errors mostly concern individual radar pixels with significantly higher reflectivity values (e.g., more than 70 dBZ) compared to the surroundings. To avoid this problem, ~~only reflectivity in the range of 35 to 70 dBZ was considered in the analyses~~ **reflectivities below 35 dBZ or above 70 dBZ were set as missing values**. Following Puskeiler et al. (2016), an additional verification and correction filter was applied **for reflectivity values of $Z > 45$ dBZ with a difference of $\Delta Z > 5$ dBZ to the adjacent pixels. The affected pixel is set to the mean value of its 8 surrounding pixels and this filter was applied to all consecutive radar scans:** ~~for values larger than 45 dBZ:~~

$$Z(x,y) = \frac{1}{8}\left(\sum_{i=-1}^{1}\sum_{j=-1}^{1} Z(x+i,y+j) - Z(x,y)\right) \quad (1)$$

In addition, a high reflectivity value **at least twice as higher compared to the 8 neighboring values** ~~occured~~ that cannot be observed in the scan before or afterward ~~only, it~~ is considered an artifact and removed.

3.2 Lightning filter

Despite the radar tracking routine (see next paragraph) has included a clutter filter, several erroneous signals are still present in the radar data. **For example, isolated non-meteorological targets such as electronic signals or reflectivities from wind turbines can emerge in radar scans (Steiner and Smith, 2002).** ~~Such high reflectivity echoes can, for example, appear when the radar beam hits lightning during a storm (Ligda, 1956; Ligda, 1996). The ionized lightning combined with high temperatures lead to a specific reflection of the transmitted radar beam to the antenna.~~ Since hail occurs only in association with thunderstorms (Baughman and Fuquay, 1970; Changnon, 1999; Wapler, 2017), lightning is expected near high reflectivity cores. In addition to the gradient filter described above, we used lightning detections to further remove artificial clutter. If high reflectivity values **occur** during a ~~day~~ **24-hour period** ~~occurs~~ without lightning, the values at the affected grid points are set to zero. A maximum distance of 10 km was chosen between a lightning discharge location and the pixels with high reflectivity. Distances of 5, 15, and 20 km were also tested; a distance of 5 km led to the disruption of several hail tracks due to gaps in reflectivity values; the other two thresholds affected the results only marginally. **An example of the lightning filter application during a hailstorm can be found in Fluck (2018) for the 27 July 2013 at 15:30 UTC.**

3.3 The convective cell tracking algorithm CCTA2D

The object-based Convective Cell Tracking Algorithm (CCTA2D) permits the reconstruction of tracks of individual convective cells using 2D radar data. The algorithm is based on the tracking algorithm TRACE3D (Handwerker, 2002), originally developed and optimized for 3D radar reflectivity from a single radar in spherical coordinates. TRACE3D was further extended to radar reflectivity data in Cartesian coordinates such as those provided by the DWD radar network (Puskeiler et al., 2016). A second version was adapted to 2D terrain-following near ground reflectivity (CAPPI) using both the RX product from DWD and the French mosaic including France, Belgium, and Luxembourg (Fluck, 2018).

The first step of CCTA2D is to identify ~~convective cells with reflectivity values of at least 55 dBZ~~, **regions of intense precipitation (ROIP) delimited by $Z \geq 35$ dBZ and to determine the corresponding maximum reflectivity values (Max$_{ROIP}$). In order** to distinguish individual ~~cells~~ **reflectivity cores (RCs) within each ROIP**, ~~using different sub-thresholds.~~ **a value of $\Delta Z = 10$ dBZ is subtracted from Max$_{ROIP}$ to set the minimum threshold necessary to delimit a single RC (Min$_{thresRC}$). Thus, the value of Min$_{thresRC}$ remains the same for all identified RCs inside a ROIP. If Min$_{thresRC}$ is less than 55 dBZ, the RC is rejected and not tracked by CCTA2D. Two additional conditions are required for a RC to be classified as a potential convective cell and to be tracked by CCTA2D: A minimal surface area of 5 km^2 is needed to define a RC with at least 3 radar bins of $Z \geq 55$ dBZ. The thresholds detailed above to identify potential convective cells in CCTA2D are summarized in Table 1.** The 55 dBZ threshold is referred to as the hail criterion according to Mason (1971), and was successfully used in several studies (e.g., Hohl, 2001,Hohl et al., 2002,Kunz and Kugel, 2015). Schuster et al. (2005), for example, found the 55 BZ to be a good indicator for damaging hail on the ground in Eastern Australia. Puskeiler et al. (2016) estimated a slightly higher threshold of 56 dBZ best separating between days with and without insured damage to buildings, but confirmed the 55 dBZ to estimate at best insured damage to crops. Categorical verification using insurance loss data over a 7-year period in southwest Germany for this threshold yields a Heidke Skill Score HSS of 0.6, a quite high value confirming the detection skill (it should be noted that this value increases to HSS = 0.71 when using an adjusted version of the Waldvogel et al. (1979) criterion requiring 3D radar data). **In the same study, Puskeiler et al. (2016) found that the Probability of Detection (POD) has reached 0.65 and the False Alarm Rate (FAR) has attained 0.4, indicating that 35% of the observed hail events are missing while 40% of those predicted events are false alarms.**

The second step of CCTA2D is the temporal and spatial tracking of all detected convective cells. The algorithm assigns the RC of the previous radar composite to the actual composite according to the estimated propagation velocity and the position of the RC. Prerequisite of the tracking is that similarities between different RCs, for example, in intensity and size, from one time step to the next must exist within a certain search radius for accurate RC assignment and tracking. The search radius is given by the estimated distance of an initial RC displaced during a time step of 5 minutes multiplied by a velocity factor of 0.6.

Special attention is given to cell splitting and merging. **Cell splitting is a prominent feature of supercells associated with vertical pressure disturbances. In most cases, the left-moving cell weakens very quickly, whereas the right-moving supercells further exist. In order to track both cells after they have been splitted, a splitting (merging) option in the tracking algorithm is necessary. Furthermore, without splitting or merging options, the physical characteristics of SCS**

Table 1. **Thresholds required in radar composites to identify potential convective cells with the CCTA2D algorithm.**

Description	Value	Units
Minimum reflectivity of a ROIP	35	dBZ
Minimum reflectivity of a RC	55	dBZ
Reflectivity to subtract from ROIP Maximum	10	dB
Minimum RC area	5	km^2
Minimum number of elements inside a RC	3	-

tracks such as their length or their angle of orientation could be incorrectly computed by CCTA2D. To detect cell splitting, the initial RC is first spatially displaced to the position of the following RC (e.g., the successor), and their respective areas are compared (Handwerker, 2002). If the area of the successor differs significantly from the initial RC, it is assigned a potential splitting. In the case of merging, the opposite calculation from cell splitting is performed. **The maximum distance between two RC centers that could merge is set to 10 km.** Initial and successor areas are then compared, and the successor is placed at the weighted center of all initially detected cores. Merging occurs when the successor area is larger than the initial RC. To avoid reflectivity core crossings or overlapping, each RC is enumerated and recorded separately.

After the construction of entire cell tracks, the composite of maximum reflectivity on a given day does not provide a smooth result, but a rather scattered product. This effect is most pronounced when the cells propagate further than their horizontal extent during a measuring interval. The faster the storms move, the more scattered is the maximum reflectivity projected on a 2D plane. This can substantially reduce reflectivity values between two scans, even though a high-intensity storm crossed the area. **A gap of reflectivity values can also appear on radar scans in regions with overlapping radar data, especially on neighboring countries such as in the Rhine Valley.** To consider this effect, an advection correction was performed following Puskeiler et al. (2016). A translation of the reflectivity cores is computed from one time step to the next considering the horizontal wind field estimated by CCTA2D along a track. ~~**Horizontal wind components**~~ **The field of motion vectors** as well as the track direction of the convective cells are computed and projected on the German and French grid. Each point along a track includes a velocity shift-vector in north-to-south $\mathbf{dv}$ and west-to-east $\mathbf{du}$ directions. **The so-called shift-vector U is denoted as:**

$$\overrightarrow{\boldsymbol{U}}(x,y) = \begin{pmatrix} du(x,y) \\ dv(x,y) \end{pmatrix} \tag{2}$$

As the CCTA2D algorithm only determines the center of a track, an n-time parallel duplication of the track is required with a vector field from all locations of the thunderstorms. The parallel shift at the position (b,c) is done with normalized vectors `t1` and `t2` of the cell motion direction with a spacing on each side of the track depending on the size of the RC and a maximum spacing of 20 km. The position (b,c) obtained from the shift vector U is calculated as

follows:

$$(b,c) = \left(x + |\frac{\delta \mathbf{t}_{1,2}}{\delta x}| \cdot n, y + |\frac{\delta \mathbf{t}_{1,2}}{\delta y}| \right) \quad (3)$$

Equation 3 thus provides a displacement field of the entire cell complex.

In our analysis, ~~Tests with~~ long-living SCS tracks were compared with hail reports archived by the European Severe Weather Database (ESWD) operated by the European Severe Storms Laboratory (Dotzek et al., 2009) along the reconstructed storm tracks to assess the reliability of CCTA2D. In fact, ~~In most cases, the ESWD reports are located close to the center of SCS tracks.~~ in the recent paper of (Kunz et al., 2020), the authors separate all SCS events used in this study from the hailstorm events by assessing the presence of hail using ESWD reports in the vicinity of SCS tracks. Out of 26 012 SCS events in total, only 985 events could be confirmed by hail reports. The main reason of this significant reduction of confirmed hail events is that ESWD reports are by far not complete. Whereas most of the reports prevail for Germany, only a low number is available for France, Belgium, and Luxembourg.

4 Results

4.1 Spatial distribution of hail

Figure 3 presents the hail probability map for the radar domain (cf. Figure 2) in terms of ~~the~~ annual average ~~number of~~ hail days during the period from 2005 to 2014 with a resolution of 1×1 km^2 based on 2D radar reflectivity. A day is considered as hail day when the threshold of 55 dBZ is exceeded in the daily maximum reflectivity composite after (i) data correction, (ii) filtering with lightning data, and (iii) tracking with the object oriented algorithm CCTA2D as described in the previous section. If the hail criterion of $Z \geq 55$ dBZ is fulfilled on a specific day at a single grid point, this grid point is set to 1, otherwise it is counted as zero. The total of all days with hail over the entire 10-year period divided by the number of years yields the radar-based "hail climatology". In accordance with other hail frequency analyses (e.g., Puskeiler, 2013, Nisi et al., 2016, Junghänel et al., 2016, Nisi et al., 2018), the term climatology is used here, even though our investigation refers to a period far below a climatological time scale of $\geq$30 years. Note that this climatology represents the spatial distribution of convective cells with high reflectivity, but not directly of hail as the 55 dBZ threshold does not guarantee hail on the ground. Similarly, the absence of high reflectivity does not ensure that hail did not occur (See Section 3.3). The term hail days used in the following parts of this study refers to the exceedance of reflectivity, but not to confirmed hail observations.

As can be seen in Figure 3, the spatial variability of hail days is very large, but some patterns with distinct minima or maxima can be identified. The lowest number of hail days is around the coasts, both the Atlantic and the Mediterranean with low frequency over northwestern France, Belgium and North Germany. Conversely, the highest number of hail days is located towards the East of France, with maxima present in contiguous area such as in central France (area MAS) or in southwestern Germany. Besides the recognizable structures of maxima and minima, some very patchy patterns appear for example in area ECG or LUX. As a result, an increasing gradient in the number of hail days can be recognized from

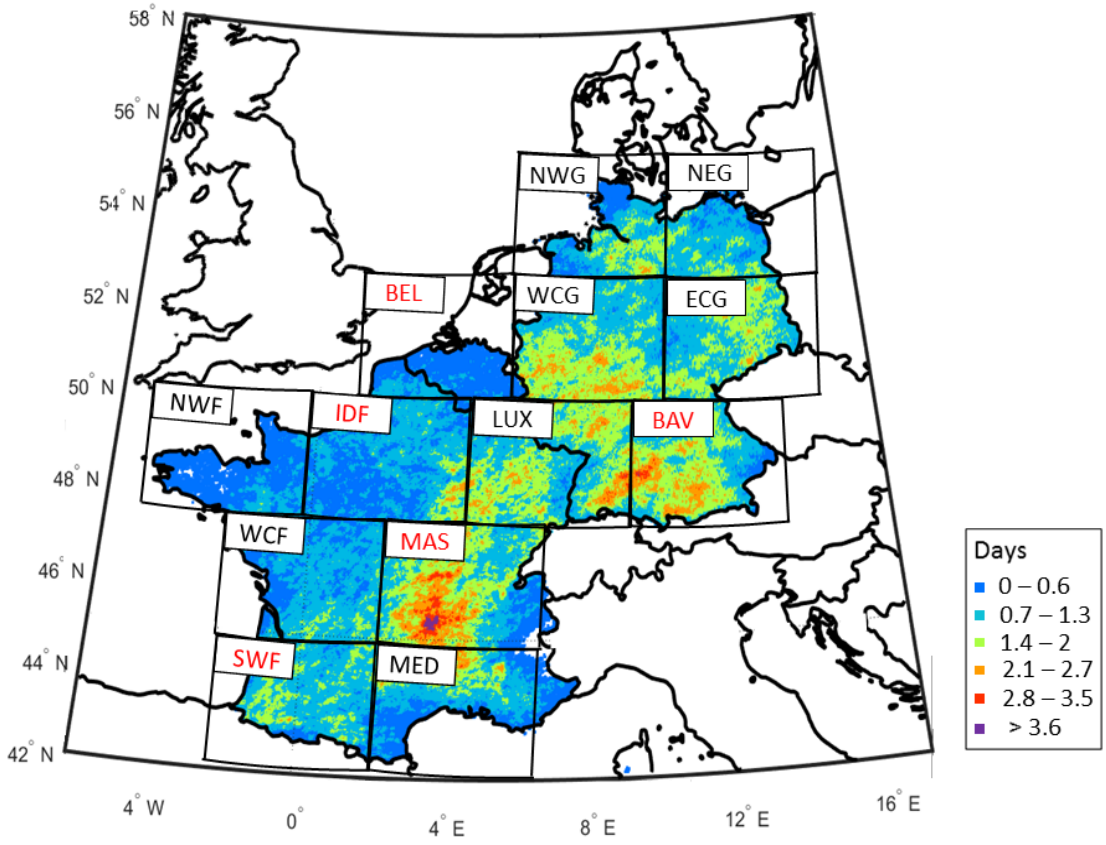

Figure 3. ~~Number of radar-derived hail days~~ **Annual radar-derived hail frequencies** for 1×1 km^2 grid points in France, Germany, Belgium, and Luxembourg between 2005 and 2014. Squares represent boundaries of subdomains further investigated in this study (See subsection 4.3 for further details). **The subdomains were named as follow: NWG (Northwest Germany), NEG (Northeast Germany), BEL (Belgium), WCG (West-Central Germany), ECG (East-Central Germany), NWF (Northwest France), IDF (Île-de-France), LUX (Luxembourg), BAV (Bavaria), WCF (West-Central France), MAS (Massif Central), SWF (Southwest France), MED (Mediterranean).** Special emphasis is given for subdomains ~~delimited~~ **written** in red.

northwestern France towards central France; and a predominant gradient pointing from North towards South Ger-
340 **many can also be mentioned.** ~~**Important is the geographical location of the Massif Central and its shape (in the continent, perpendicular to the dominant flow). It is the first natural barrier from the Mediterranean, and air flow advected from there can transport warm and moist air along the Rhone Valley, by channeling and accelerating along valleys situated southeast of the Massif Central. These valleys are oriented on a northwest-to-southeast axis and permit the Mediterranean flow to circulate along the entire valley (Bastin et al., 2005) The Massif Central can also be affected by a~~

~~cold low-level wind (mistral) coming from northwest to southern directions and transporting dry and cold continental air over the Limagne Plain, thus leading to blocking at the windward side of the foothills of the Livradois and Aubrac mountains, where hailstorms frequently occur.~~

A close-up investigation of the hail hot spots **is detailed hereafter.** ~~can be found in~~ **Figure 4 represents the location of the mean hail days overlaid with the 10 m mean wind during hail days (in terms of speed and direction) from 2005 to 2014 on the high-resolution global relief ETOPO1 having a 1 arc-minute resolution (Amante and Eakins, 2009). The 10 m mean wind was computed using the hourly and 31km horizontal resolution ERA5 global analysis (Hersbach et al., 2020).**

The area with the highest average number of hail days during the 10-year investigation period is situated **on the leeward side of the highest mountains of the Massif Central averaging up to** ~~46~~ **4.6 hail days.** ~~in central France on the northern flank of the Massif Central accumulating on the southwestern flank of the Livradois situated between the Aubrac and the Forez mountains.~~

This maximum extends over the central part ~~extending~~ **over a few kilometers of the Massif Central (named Livradois region), composed by a plain and middle-range mountain measuring up to 1200 m high (named Livradois mountains). During days with hail, a strong flow is coming from the Mediterranean Sea with a northern direction, thus impinging the southern and southeastern mountains of the Massif Central at a sharp angle. Another general westerly flow reaches the western part of the Massif Central. Interestingly, it seems that not only the location of the Massif Central is responsible for the increased number of hail days downstream, but also the flow convergence where the westerly flow meets with the flow coming from the Mediterranean. One may speculate that even without the Massif Central hail days might be increased in that area of low-level flow convergence. The large valleys on the western side of the Massif Central, oriented from southwest to northeast, facilitate the passage of the flow coming from the southwest into the Livradois region. This region with an average number of 3.2 hail days per year is located in an area where the wind vectors converge both in the direction and velocity. In order to better understand the flow characteristics over the Massif Central shown in Figure 4, we calculated the Froude number on radar-derived hail days from ERA5 (Queney, 1948; Smith, 1979) for a region covering the Massif Central entirely and ranging from 44.0° to 46.5°N and from 2.0 to 4.7°E. The Froude number is calculated as follows:**

$$Fr = \frac{U}{NH} \tag{4}$$

where U represents the wind speed perpendicular to the mountain and was computed by applying a density weighted integration over the lowest 2000 m. H is a characteristic mountain height set to 1300 m for the Massif Central region and N is the Brunt–Väisälä frequency. According to Huschke (1959), the squared Brunt–Väisälä frequency N^2 is defined as :

$$N^2 = \frac{g}{\theta_{va}} \frac{\partial \theta_{va}}{\partial z} \tag{5}$$

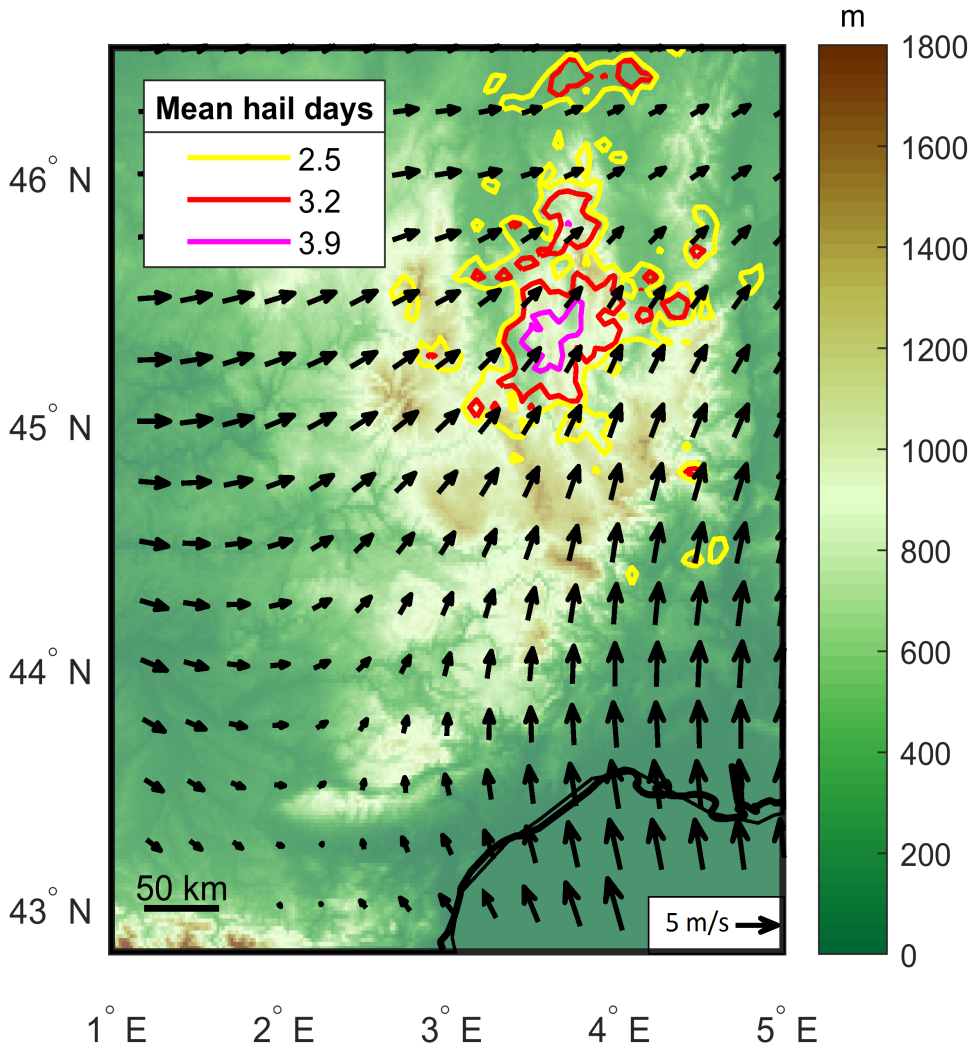

Figure 4. Contours of ~~radar-derived hail days~~ **the average number of hail days** from 2005 to 2014 overlaid with the orography **and the 10m mean wind flow during hail days**.

Where g is the gravitational acceleration equal to 9.8 m.s^{-1}, θ_{va} is the ambient virtual potential temperature, and $\frac{\partial \theta_{va}}{\partial z}$ represents the vertical gradient of the virtual potential temperature. In our analysis, we considered the root-mean-square of the Brunt–Väisälä frequency N in order to exclude imaginary values.

The mean Froude number on hail days over the Massif Central from 2005 to 2014 is $Fr = 0.39 \pm 0.3$. According to Smith (1979) and Smolarkiewicz and Rotunno (1989), a Froude number below 1 suggest a flow that goes around the mountain rather than directly over it. Thus, it can be assumed that the flow around the Massif Central is deviated by

the mountains peaks leading to convergence downstream at low levels on the leeward side of the Massif Central, where the hail hot spot is located.

Several authors have found an increased hail frequency rather downstream than upstream or directly above the mountains. This is for example the case in the Pyrenean region (Vinet, 2001, Berthet et al., 2011, Hermida et al., 2013, Merino et al., 2013), near the Black Forest in Germany (Kunz and Puskeiler, 2010, Puskeiler et al., 2016), or in the vicinity of the Alps (Eccel et al., 2012, Nisi et al., 2018). In a review about orographically induced convection, for example, Kirshbaum et al. (2018) found that leeside convergence produces ascent required for convective initiation on the leeward side of mountains by referring to the studies of Mass (1981) about lee-side convergence near the Olympic mountains in the Washington State and of Barthlott et al. (2016) on convection initiation near Corsica mountains during HyMeX (Hydrological cycle in the Mediterranean eXperiment). Low-level flow convergence could explained the high frequency of hail on the leeward side of the Massif Central; however, this is still a hypothesis that require additional observations and numerical simulations in this region to assess convection initiation.

~~**The location of the latter maximum shows an interaction between several factors that result in the triggering of hailstorms in that specific region.**~~

~~**The strength of the updrafts depends on the diurnal thermal circulation (and, of course, the terrain's slope).**~~

~~**During the afternoon, the flow may go along the Aubrac Mountains and along the slopes of the volcanoes (Chaîne des Puys) located on the western flanks of the mountain range.**~~

~~**The air that is forced to flow over the higher mountains may generate generates gravity waves on the leeward side of the mountain (Chappell, 1986), an area of lower pressure, enhanced turbulence, and periodic vertical displacement of fluid parcels. The combination of increased vertical wind shear due to flow deviations at obstacles, and low-level flow convergence, and increased moisture at lower levels may lead to favorable conditions for the triggering of convection downstream of the mountains (Kunz and Puskeiler, 2010)**~~

The northeastern part of France, including the regions of Burgundy (referred to as region 9 in Figure 1), Champagne-Ardenne (region 6), Alsace (region 8), Lorraine (region 7) and Franche-Comté (region 10) ~~**(Figure 1)**~~, are affected with a maximum of ~~**31**~~ **3.1** hail days in the central part of Burgundy, and more precisely on the eastern side of mountains ranging from approximately 300 to 900 m. ~~**(named Morvan range)**~~. In Champagne-Ardenne, ~~**the region flanking Burgundy on its northeast boarder**~~ the number of hail days reaches up to ~~**29**~~ **2.9** days over the mainly rolling terrain. In Lorraine, where the terrain is almost flat and the climate is more continental, on average ~~**27**~~ **2.7** hail days were counted in its central part. A local and ~~**weaker**~~ **lower** maximum of ~~**24**~~ **2.4** hail days can be recognized in South Alsace ~~**at the southeast edge of Lorraine on the windward side of the Vosges mountains (mentioned as D in Figure 1**~~ , representing an area with complex terrain with mountains up to 1.424 m agl. ~~**(Grand Ballon). The north-to-south orientation of the Vosges in addition to the higher elevations in the southern part represent a natural obstacle opposed to the main southwesterly flow, and may help convective clouds to develop in southwestern Alsace**~~ Another hail hotspot in the northeastern part of France is found along the northern ridge of the Jura Mountains (mentioned as E in Figure 1) in Franche-Comté with ~~**25**~~ **2.5** hail days. ~~**The western part of the region is mainly flat and includes the Doubs Valley.**~~ Note that the Jura mountains represent a natural obstacle frequently

~~may~~ triggering thunderstorms **(Piper and Kunz, 2017)** and hailstorms by orographical lifting **(Langhans et al., 2013, Schemm et al., 2016, Nisi et al., 2018 among others).**

The Rhone-Alpes (referred to as region 11 in Figure 1) is a region likewise frequently affected by hail. This region contains the large Rhone valley and is bordered by the Massif Central in the west and by the Alps to the east. The southwestern part as well as the southeastern edge of the region show a local hail maximum with up to ~~31~~ **3.1** hail days. The existence of these two hot spots may be explained by their proximity to the Mediterranean as during southerly flows, warm and moist air is advected preferably through the Rhone valley. The warm and moist air can then be lifted, for example, near a front system crossing the country from northwest to southeast, leading to forced convection. **This effect was confirmed by Schemm et al. (2016), who analyzed the relation between radar-based hail streaks over Switzerland and adjacent regions and cold fronts identified in high-resolution model data (COSMO-2; Steppeler et al., 2003, Jenkner et al., 2010) during a 12-year period (2002 to 2013). The authors found that around 45 % of the detected hail cell initiations located on the windward side of the pre-Alps (in the Rhone valley) are associated with cold-fronts coming from the West during the summer months (May to September).**

Southwestern France, including both the Aquitaine and Midi-Pyrenees regions (referred to as regions 12 and 13 in Figure 1), is also frequently affected by hail with up to ~~26~~ **2.6** hail days in the southwest range of the Massif Central. Aquitaine and Midi-Pyrenees regions are the two regions well known in the literature for their high hail probability (Vinet, 2001, Punge et al., 2014). Hermida et al. (2015) ~~recently~~ used data from the ANELFA (Association Nationale d'Etude et de Lutte contre les Fléaux Atmosphériques) hailpad network and found that the Gers Department, located on the west side of the Midi-Pyrenees region, is the area the most affected by hail in southwestern France. ~~Finally, the~~ The western and northern sides of the Pyrenees are also frequently affected by hail with up to ~~25~~ **2.5** hail days. ~~Although the leeward side of the mountain range shows an increased hail frequency, the hail potential in the central parts is very low with around 2 hail days close to the summits of the Pyrenean mountain range.~~ According to Berthet et al. (2011), hail in that region frequently occurs when a low-pressure system is located over the western part of Spain leading to southwesterly flow over France associated with the advection of warm and moist air over the Pyrenean mountain range.

In Germany, the main hail hotspot is located in the Southwest in the federal State of Baden-Württemberg (referred to as region 4 in Figure 1), specifically over the Swabian Jura (mentioned as B on Figure 1), south of the city of Stuttgart, with a maximum of ~~31~~ **3.1** hail days. This hotspot has already been identified in previous studies of Puskeiler (2013) and Junghänel et al. (2016). **Using equation 4, we found a Froude number of $Fr = 0.51 \pm 0.6$ for 207 hail days during the period 2005 to 2014 for a region covering 48° to 49.2° N and 7.8° to 10.5° E, including the Swabian Jura as well as the Black Forest and considering a maximum elevation of 1400 m for the entire area. The Froude number found in our study in the southwestern part of Germany matches the results of Kunz and Puskeiler (2010) who estimated a Froude number for a region covering the Vosges mountains, the Rhine valley, the Black Forest and the Swabian Jura ~~below 1~~ of $Fr = 0.32 \pm 0.15$ for 65 haildays (1997—2007) using radiosondes at 12 UTC. ~~in this region, indicating~~ This low Froude number suggests** a flow-around regime of the southern and northern mountains of Black Forest causing a zone of horizontal flow convergence downstream. This convergence zone coincides with the area of the highest number of hail days (Kunz and

Puskeiler, 2010; Koebele, 2014). Moreover, Kunz and Puskeiler (2010) hypothesized that the southwesterly flow meets the Swabian Jura at a very sharp angle, which reduces the Froude number considerably and align the wind parallel to the mountain chain. This flow modification is assumed to be responsible for the flow convergence at low levels as was also found in model simulations using COSMO-DE by Koebele (2014).

Another local maximum of up to 2.6 hail days is found North of the Alps, on the western part of the State of Bavaria (referred to as region 5 in Figure 1). This result is in good agreement with the conclusion of Nisi et al. (2018) who found that this region can be affected by around 3 hail days (2002—2014). ~~**A weaker hail frequency maximum with a mean of 11 1.1 hail days are found North of the Alps in the State of Bavaria is located in the Eastern part of Bavaria. The north-to-south orientated Pre-Alpine valleys may lead to flow deviations and low level convergence, similarly to the Swabian Jura area. Also Alpine pumping, a secondary mountain-plain circulation (Weissmann et al., 2005) leading to flow towards the Alps and creating convergence zones, may play a decisive role for this distribution (Nisi et al., 2018).**~~

In the northeast of Germany, a local maximum of up to ~~**32**~~ **3.2** hail days is positioned over the Saxon Ore Mountains (referred to as A in Figure 1) South of the city of Dresden. Note, however, that this maximum is mainly caused by a high number of SCS in the year of 2007 (Piper, 2017), which was characterized by frequent upper air troughs over Western Europe and ridges over Central Europe **(Wernli et al., 2010)**, leading to high-pressure gradients on the eastern part of Germany in combination a southeast-to-northeast flow regime from the Czech Republic (note that the almost same situation occurred in 2019).

The northwestern part of Germany, including the States of Hesse (region 2 in Figure 1) and Rhineland-Palatinate (region 3 in Figure 1), and the southern part of North Rhine-Westphalia (region 1 in Figure 1) are regions affected by approximately 1.4 hail days on average. The location of the hail patterns is partly caused by the local orography with a pronounced maximum in North Hesse that lies directly on the leeward side of the Westerwald low mountain range, which is characterized by rolling terrain.

~~**In contrast to the various hail hot spots located exclusively in the continental domain and preferably along the mountain's foothills, most of the minima are found along the coastlines, where hail is also a year-round phenomenon (Dessens, 1986). Hail is rare along the Atlantic as well as the Mediterranean coasts, in the latter case only 0.2 hail days. The large heat capacity of the water reduces the diurnal temperature cycle leading to a decrease in the lapse rate magnitude. As a result, the sea contributes to the inhibition of SCS development, even if the increased moisture content of the atmosphere near the coasts provides a source of energy for the storms (Piper and Kunz, 2017).**~~

4.2 Annual variability

The frequency of SCS ~~**, respectively,**~~ shows a very large annual and multi-annual variability (e.g., Puskeiler et al., 2016; Nisi et al., 2018). This variability is partly related to large-scale flow mechanisms such as the presence of specific northern Hemisphere Teleconnection patterns representing the low-frequency mode of the climate system (e.g., North Atlantic Oscillation, NAO, or East Atlantic pattern, EA) or by variations in the sea surface temperature (Piper et al., 2019). Having reconstructed a

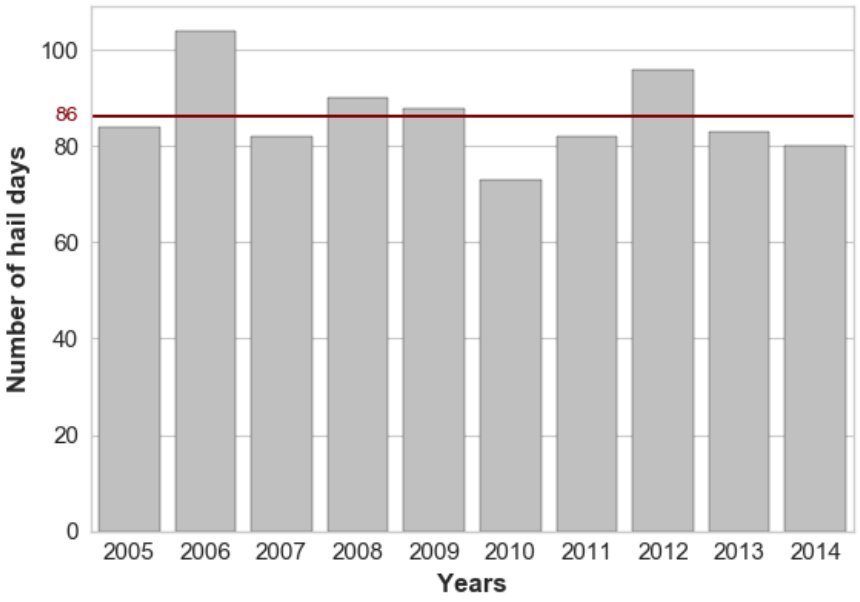

Figure 5. ~~Anomalies of annual mean~~ **Yearly number of** hail days ~~with respect to the overall mean of hail days~~ from 2005 to 2014. **The red line indicates the overall mean of hail days from 2005 to 2014.**

very large event set of SCS/hailstorms as presented in the previous section, we are also interested how the frequency of these events vary across the whole domain and regionally.

~~Annual mean frequency anomalies were computed by averaging all hail days over the entire investigation area for each year between 2005 and 2014 (Figure 5). and subtracting the mean number of hail days of the entire period.~~

~~Positive or negative values represent higher or lower numbers, respectively, of hail days compared to the 10-year average~~ ~~As shown in Figure 5 the annual variability is very high.~~ ~~and without any trend.~~ Averaged over the entire investigation area, the annual number of hail days is between 72 (2010) and 103 (2006) with a mean of 86 (Figure 5). In 2006, large parts of Europe, including Germany, Belgium, Luxembourg, and northwest France, experienced higher temperatures than on average, especially during the end of June and July **(NOAA, 2007)**, where two (moderate) heat waves occurred (Fouillet et al., 2008). As a result, the sea surface temperature over the Mediterranean showed a positive anomaly (**NOAA, 2007, Lenderink et al., 2009**), leading to intense evaporation rates and, consequently, to an increase in the amount of water vapor in the atmosphere **(Chaboureau et al., 1998)**. ~~In addition, large-scale lifting (e.g., related to differential vorticity advection) could have led to an increase in convective available potential energy (CAPE) and a low convective inhibition (CIN). The combination of high moisture in the boundary layer, low CIN, high CAPE and lifting mechanisms~~

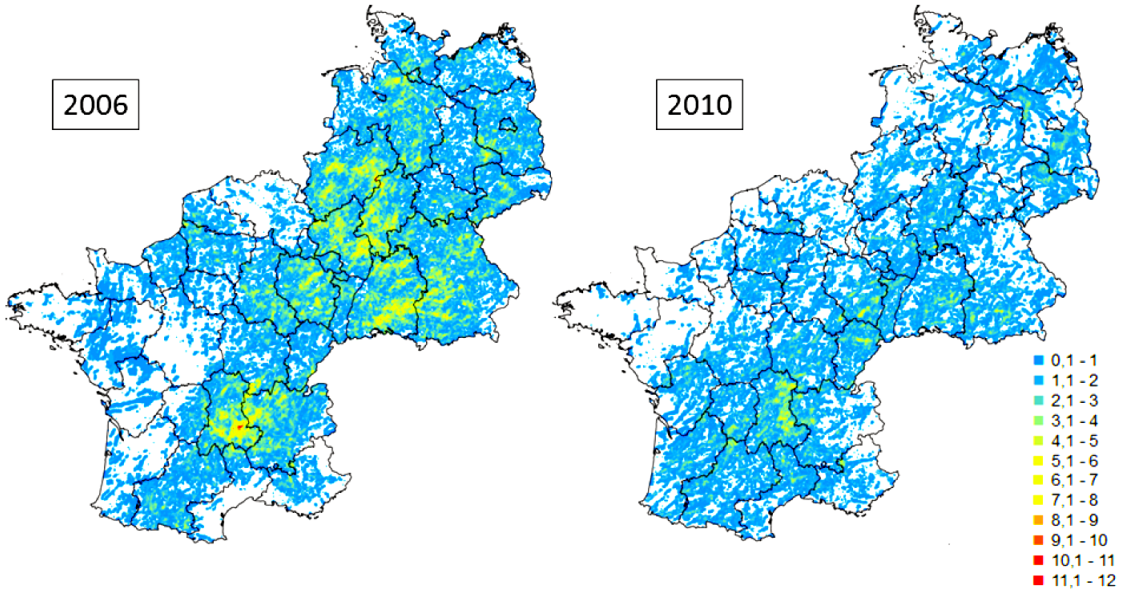

Figure 6. Number of radar-derived hail days exemplary shown for the years with the highest (2006, left) and lowest (2010, right) hail day frequency.

~~may give rise to a substantial increase in SCS.~~ The spatial distribution of hail days in 2006 (Figure 6) strongly resembles the climatology, with several maxima near hilly terrains and minima near the coastlines. Some hot spots can also be detected over the northwest part of France and in southwestern Germany.

The year with the second highest number of hail days, 2012, was dominated by an episode with intense thunderstorm activity over southwestern Germany and France during the end of June and in July (DeutscheRück, 2013).

Even though the year of 2010 showing the lowest number of hail days was very warm on the global scale (NOAA, 2011), summer temperatures over large parts of Europe including Germany were below average. Furthermore, several persistent large-scale ridges occurred during the summer, which may have suppressed the formation of SCS (DeutscheRück, 2013). No clear spatial pattern can be found in this year with only a few hailstorms in Central France. Almost no hailstorm could be detected in an arc spanning from northwestern France to northern Germany. There are further regions where hail was less present compared to the mean of 2010, including entire Belgium, Luxembourg, and the northwest of France, especially Normandy, Brittany and the coastlines. Interestingly, the year of 2013 likewise shows a negative anomaly in the number of hail days even if at the end of July two supercells associated with the low pressure Andreas caused an unprecedented economic loss of EUR 3.6 billion in several densely populated areas of Germany (Kunz et al., 2018).

4.3 Seasonal and diurnal cycles of SCS

The large spatiotemporal variability of hail discussed in the previous sections leads us to the question of the seasonal and diurnal cycle of SCS at the regional level. For this purpose, the entire study area is divided into 13 subdomains of similar size (around 75,000 km^2) framed in Figure 3. **We selected five subdomains with different terrain and climatological characteristics for further discussion: Belgium (BEL), Ile-de-France (northern France; IDF), Bavaria (southeastern Germany, BAV), the Massif Central (central France; MAS), ~~and Aquitaine (W France, MAQUI),~~ and Southwest France (SWF).** Subdomains ~~**NBEL**~~ **BEL**, ~~**MAQUI**~~ **SWF** and IDF, have a climate strongly influenced by maritime air masses. Among them, subdomains ~~**NBEL**~~ **BEL**, and IDF represent flatlands, while subdomain ~~**MAQUI**~~ **SWF** contain the high mountains of the Pyrenean. Subdomains ~~**BAVAR**~~ **BAV** and ~~**MCEN**~~ **MAS** both have a rather continental climate, but have a different orography: While mainly hilly terrain characterizes subdomain ~~**BAVAR**~~ **BAV**, subdomain ~~**MCEN**~~ **MAS** comprises the higher mountains of the Massif Central.

To quantify the number of hail days in each subdomain, ~~**the number of hail days**~~ **a 10-day moving average of the number of hail days** was ~~**accumulated**~~ **calculated for the period 2005 to 2014** (**Figure 7**). Despite the large variability seen in the seasonal cycles of the subdomains considered, some similarities can be recognized. All time series of the different subdomains feature a clear annual cycle with a minimum of hail days in spring and autumn and a maximum during the summer. This characteristic cycle with a strong increase in the hail day frequency during April/May, a significant decrease around September, and with a maximum during the summer months was found by several other authors such as Dessens (1986) and Vinet (2002) for France, Belgium and Luxembourg, Gudd (2003), Deepen (2006), Mohr and Kunz (2013) and Puskeiler et al. (2016) for Germany, and Nisi et al. (2014) and Nisi et al. (2018) for Switzerland and northern Italy.

The mountainous subdomain ~~**MCEN**~~ **MAS** shows the largest **average** number of hail days and has the most pronounced annual cycle. Until the end of April, the **average** number of hail days for the 10-day running mean is below ~~**200**~~ **10**. During May and beginning of June, the number increases substantially from ~~**281**~~ **9** around May 10 up to ~~**453**~~ **17** days on June 9. The more pronounced diurnal temperature cycle for continental regions, associated with a higher lapse rate in combination with orographic lifting, may explain this increase (Berthet et al., 2011). After June 9, the average number of hail days increase steadily until to reach the overall maximum for the MAS region at the end of July with ~~**531**~~ **23** days.~~**The higher lapse rate associated with the peak in solar radiation during long daytime in the summer combined with southwesterly flows, advection of moist and warm air, and orographic effects may explain the peak (Ludlam, 1980, Punkka and Bister, 2005, Changnon and Changnon, 2000). After the maximum, the average number of hail days decreases slightly during the end of the summer.**~~

Subdomain IDF likewise show a high hail frequency during the summer with up to ~~**271**~~ **14** days, mainly at the end of July. This subdomain is under the influence of the Atlantic Ocean (Cantat, 2004), leading to an increased frequency of troughs (Vinet, 2001, Berthet et al., 2013). ~~**This domain also is characterized by complex terrain such as the low Parisian Basin compared to the upper part of the arc-shaped Massif Central with higher terrain gradients that may explain the**~~

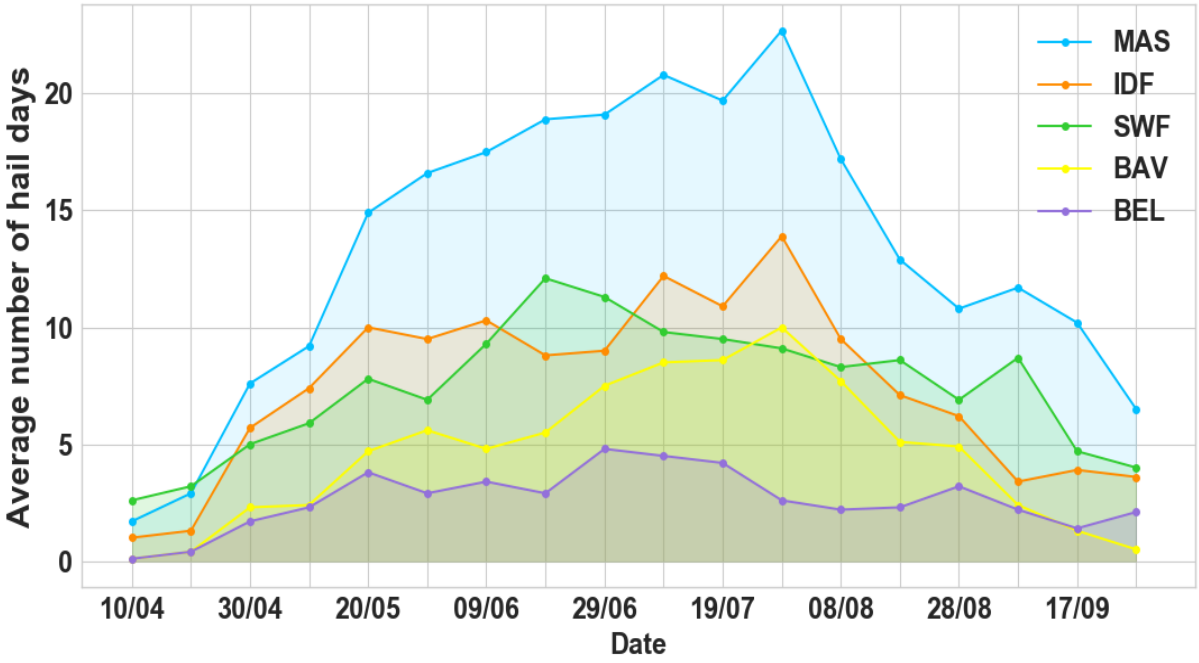

Figure 7. Time-series of **the mean number of** radar-derived hail days (10-days moving average ~~**denoted as counts**~~) for the subdomains ~~**NBEL**~~ **BEL**, IDF, ~~**BAVAR**~~ **BAV**, ~~**MCEN**~~ **MAS** and ~~**MAQUI**~~ **SWF** shown in Figure 3.

~~**contrast between the hail-peak located over the Massif Central, which is approximately twice as high compared to the peak nearby the Morvan.**~~ Within this subdomain, the number of hail days increases slightly until the peak with a first local maximum in the middle of May (around ~~**200**~~ **10** hail days) and a second local maximum at the beginning of July with around 12 hail days. Spring hailstorms may be associated with subtropical air masses coming from Spain, while summer storms preferably form ahead of cold fronts (Berthet et al., 2011). The number of hail days decreases sharply from the hail-peak season toward the end of September.

Subdomain ~~**MAQUI**~~ **SWF**, located in the very southwest of France, has a very broad hail peak in the middle of June with ~~**214**~~ **12** hail days during the 10-day moving average centered around June 19. Afterwards, the number slightly decreases, thus showing a right-skewed distribution. This maximum found in June differs from the analysis of Dessens et al. (2015), who found that May is the most active month followed by July over the southwestern part of France and the Mediterranean area (situated along the Rhone valley). Also Fraile et al. (2003) and Hermida et al. (2013) found that May is the month with the highest hail kinetic energy in southwestern France. Reasons for this discrepancy can be due to a longer period analyzed by Dessens et al. (2015), while Hermida et al. (2013) and Fraile et al. (2003) focused on a time range starting from the 90s. Furthermore, the scattered network of hail pads is denser near the subdomains influenced by maritime air mass.

Subdomain ~~BAVAR~~ BAV, located in Southeast Germany, has the maximum of hail days at the end of July, later in the year than the other subdomains. ~~This peak occurs when convective activity due to local conditions (local winds, uplifts) and larger-scale conditions (e.g., temperature advection) are the highest (increase of wind shear, low-level convergence).~~ Kunz and Puskeiler (2010) and Puskeiler (2013) also found that July is the month with the highest number of hail days in central and southern Germany. ~~Interestingly, the number of hail days remains almost constant between the beginning of June and mid-August.~~ Subdomain ~~NBEL~~ BEL, covering the North of France as well as the upper western part of Belgium, peaks at the end of June. ~~Northern France and Belgium have a maritime climate influenced by the North Sea, with colder summers. Furthermore, sea-breezes and associated flow convergence zones may explain the peak at the beginning of the summer. In Belgium, sea-breezes preferably occur in spring or summer (Damato et al., 2003), when the temperature difference between land and ocean is most significant.~~ A 10-year radar-based climatology conducted for Belgium by Lukach and Delobbe (2013) confirmed May and June to be the most favorable months for hail.

The diurnal cycle of hailstorms shown in Figure 8 represents the times where the CCTA2D detects the first radar reflectivity of 55 dBZ or more. Since the local time (LT) varies through Europe with approximately one hour from Brittany in France to Saxony in Germany, all times originally given in UTC are converted to LT, representing four minutes per degree of longitude. In all subdomains, hail occurs most frequently in the afternoon between 13 and 18 LT, while between midnight and 10 LT the fewest events are detected (Figure 8).

Some discrepancies appear in the daily cycle, mainly depending on the location and characteristics of the respective subdomain. For example, the frequency of hailstorms in ~~NBEL~~ BEL situated along the North Atlantic (but also in ~~l~~ other subdomains located roughly North of latitude 48 °N and Mediterranean coastlines; not shown) reveals a large increase during the afternoon (14-15 LT) and a slow, but gradual decrease toward the morning.

In contrast to the subdomains located in the northern part of Europe, domains ~~MCEN~~ MAS over the Massif Central and SWF in South France peak one hour later at around 16 LT. The peak during the late afternoon for more continental regions is presumably due to local orographic effects, such as slope or valley winds (Nesbitt and Zipser, 2003).

For subdomain ~~MAQUI~~ SWF, located in southern France between the Atlantic Ocean and the Pyrenees Mountains, the average number of hail days reminds high in the late evening (20 to 22 LT). ~~This may be related to the natural barrier of the Pyrenean Mountains, which may block convective storms from reaching that subdomain suppressing hail formation on the southern foothills of the mountains during the afternoon (Kirshbaum et al., 2018, Berthet et al., 2013). On the northern foothills of subdomain MAQUI, flow convergence associated with local winds may lead to the formation of updrafts. Another~~ A plausible effect is that severe storms may develop from pre-existing scattered thunderstorms that form during the afternoon as was found by Nisi et al. (2016) and Nisi et al. (2018). This feature might be decisive for the hailstorm maximum in the evening in the canto of Ticino in southern Switzerland.

Some literature exists regarding the diurnal cycle of hail in Europe (Punge and Kunz, 2016). Bedka (2011), for example, recognized a diurnal cycle of overshooting tops that is related to the presence of orography and/or to the distance to the sea. Kaltenböck et al. (2009) found a peak in hail occurrence in the middle of the afternoon through Europe. ~~This is also the case in Poland (Twardosz et al., 2010) or in Macedonia (Dimitrievski, 1983) where the peak is reached between 14 and 17 LT.~~

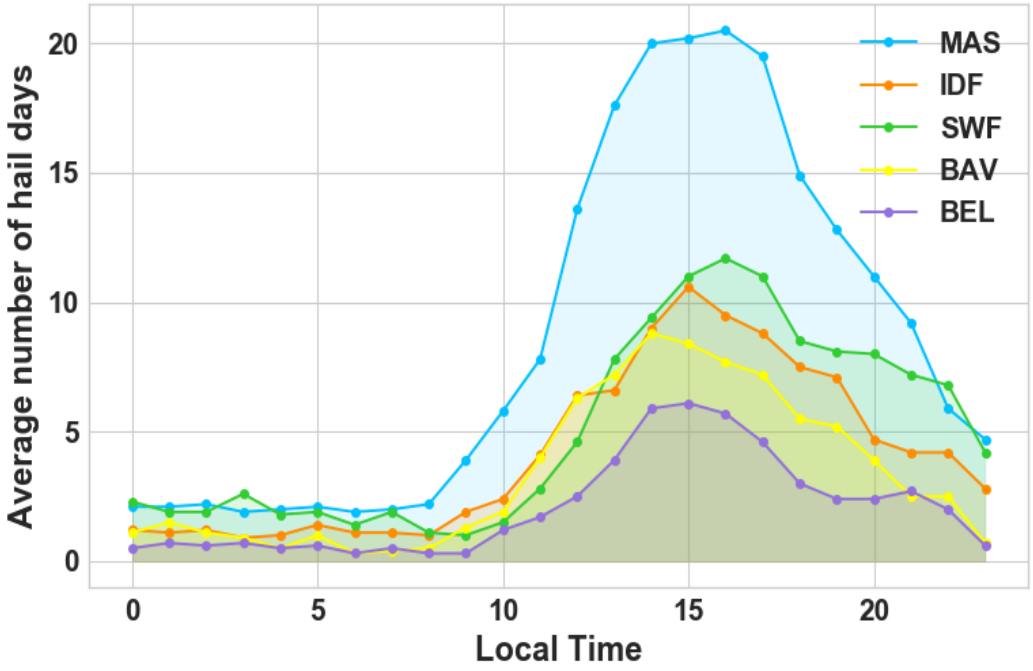

Figure 8. Hourly distribution of **the mean number of** radar-derived hail days for each subdomain.

~~**According to Martín et al. (2010), hail maximum in Spain occurs between 15 and 18 LT.**~~ Kunz and Puskeiler (2010) identified for southwestern Germany a maximum in the number of damaging hail events during 13 and 18 LT. The same peak is found in Alpine regions such as Italy (Morgan, 1973) or Switzerland (Nisi et al., 2016), where the maximum of hail occurs in the late afternoon and the minimum in the morning according to radar data analysis. Lukach et al. (2017) demonstrated for southeast Belgium that hail falls mostly during 15-16 UTC, which is in accordance to the daily cycle in subdomain BEL that includes Belgium. As for subdomain SWF in this study, Mallafré et al. (2009) found a peak later in the afternoon, around 18 LT.

4.4 First radar detection of SCS

To compare the spatial distribution of hailstorms during the night and day and to distinguish between mechanisms triggering nighttime events and convection being triggered within the boundary layer occurring preferably in the afternoon and early evening, we spatially analyzed the first detected signal of the radar-derived hailstorm tracks (hereinafter referred to as track onset). Figure 9 shows exemplary the **temporal evolution of the** spatial distribution of track onsets ~~**at 02 LT and 18 LT**~~ **grouped into 3 hour intervals**. As expected already from the daily cycles presented in Figure 8, the occurrence probability during the night is much lower than during the day (**for example** ~~**227**~~ **573** onsets were detected from 2005 to 2014 ~~**at 02LT**~~

610 **during 0 LT and 3 LT** compared to more than ~~**750 at 18LT**~~ **2670 during 15 LT and 18 LT**). Furthermore, during nighttime **(0-3 LT and 3-6 LT)**, the location of the onsets spreads more or less randomly along coastlines and the continent without any recognizable structure. Local-scale flow effects such as sea breezes may affect the triggering of convective cells near the coastlines, which may be reinforced over the Mediterranean as well as the Atlantic coastlines (Simpson, 1994). **The morning at 6-9 LT and 9-12 LT experiences more onsets compared to the nighttime with some event clusters over the northeastern**
615 **part of France or near the Massif-Central.** ~~**In contrast, onsets at 18LT**~~ **During the day and the afternoon (12-15 LT and 15-18 LT), the track onsets** form several patterns particularly near mountains, such as the Massif Central, the pre-Alpine domain in southern Germany, or near the French Pyrenees. Local effects, such as low-level flow convergence, and orographic effects, combined with large-scale features (fronts, large-scale lifting), may contribute to the reinforcement and development of convective cells near the mountain ranges **(Kunz and Puskeiler, 2010, Berthet et al., 2011, Koebele, 2014, Kirshbaum**
620 **et al., 2018)**. **During the evening (18-21 LT), the track activity is still high, especially near mountain ranges. In contrast, inland regions and coastlines are less affected by hail events compared to the day. A substantial drop in the number of track onsets occurs during the night (21-0 LT), with only a few scattered onsets in southwestern France and near the Massif-Central.**

4.5 Main characteristics of hail tracks

625 In the following section, we explore the main characteristics of our sample of radar-detected hail tracks. The length is defined as the distance in kilometers between the start and the end of a track determined by CCTA2D, i.e., the period where a threshold of 55 dBZ is reached or exceeded. The distribution of the lengths shown in the histogram in Figure 10 approximately follows an exponential function with a maximum for the first class.

In general, the mean length (with standard deviation) is 41.5 $\pm$ 36.4 km with a median of 29.5 km for the entire investigated
630 area. The tracks reconstructed for Germany have a mean length of 39.1 $\pm$ 33 km and a median of 27 km whereas in France, the mean length is slightly larger with 43.9 $\pm$ 39.8 km and 32 km for the median. In total, 43% of all recorded storms over Western Europe have a length between 1 and 10 km. The number of tracks having a length **L** between ~~**10.1**~~ **10** and 20 km decreases to 19% of the overall sample. ~~**After that, the occurrence of storms possessing longer lengths decreases slightly.**~~ Approximately 30% of all tracks have a length between ~~**20.1**~~ **20** and 150 km, and less than 8% are greater than 150 km (not
635 shown). Longer tracks can be expected for highly-organized convective systems, such as ~~**MCS**~~ **MCSs**, ~~**including squall lines,**~~ or supercells.

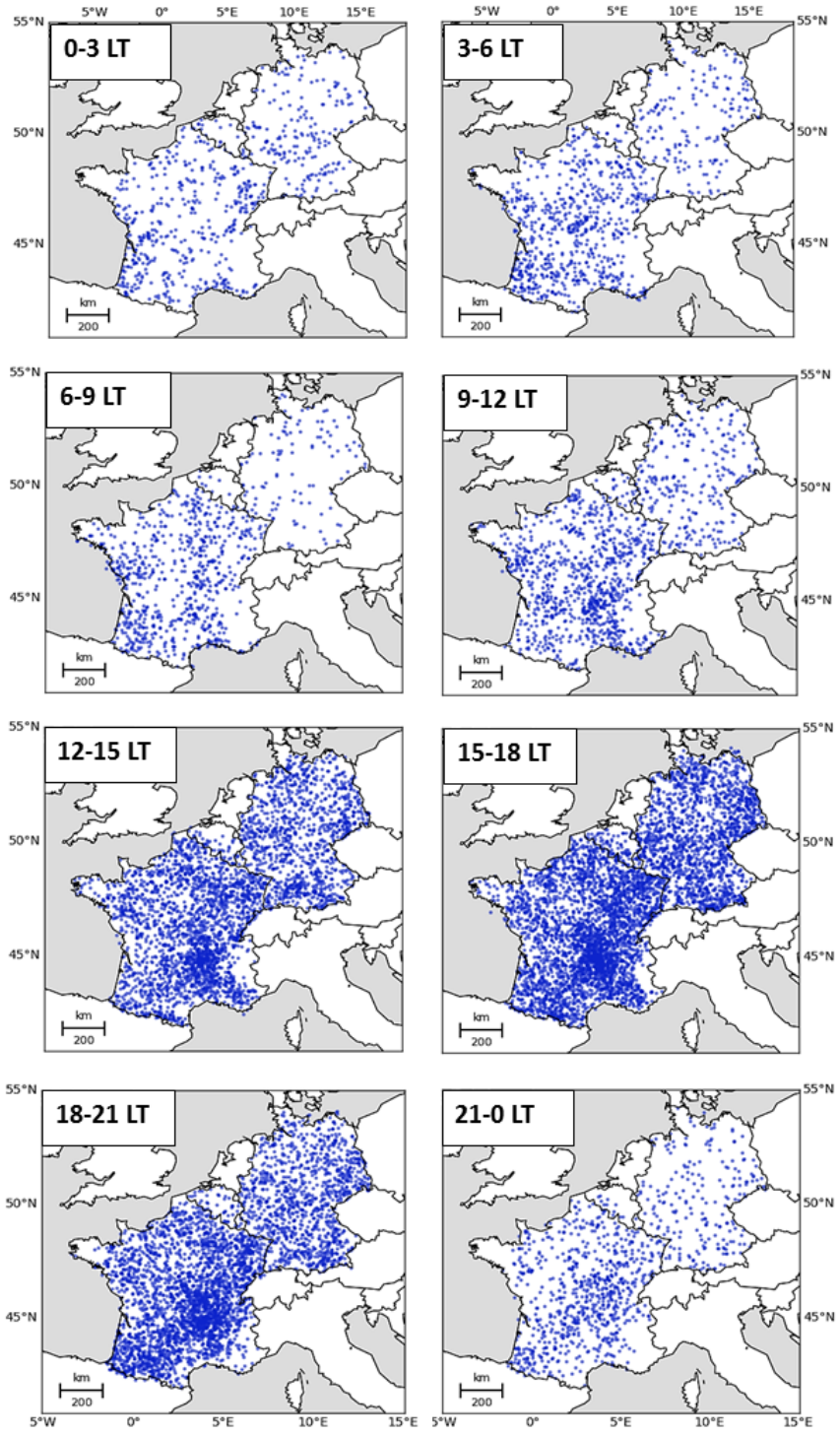

Figure 9. Locations of the first convective signatures detected by CCTA2D ~~at 02LT (A) and 18LT (B)~~ **at the indicated Local Time (LT)**.

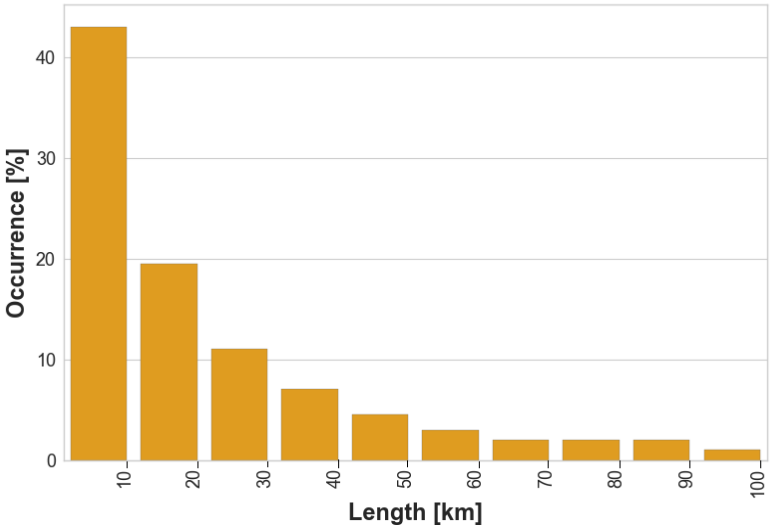

Figure 10. Histogram of all SCS mean length.

~~**(A) and mean orientation (B).**~~

Only a few authors have analyzed hail tracks characteristics in West Europe, and only very few studies based their investigations over a sufficiently long period. Puskeiler (2013), for example, investigated hail tracks lengths using 3D radar data in Germany during 2005 and 2011 and found a mean length of 48 km with a strong decrease for longer streaks, inducing a high standard deviation of 46.7 km and a median of 40 km.

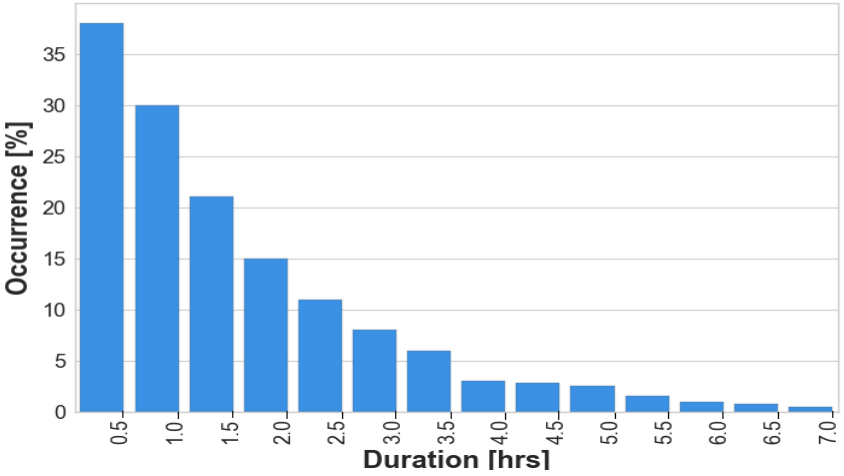

Figure 11. Same as Figure 10 but for the mean duration.

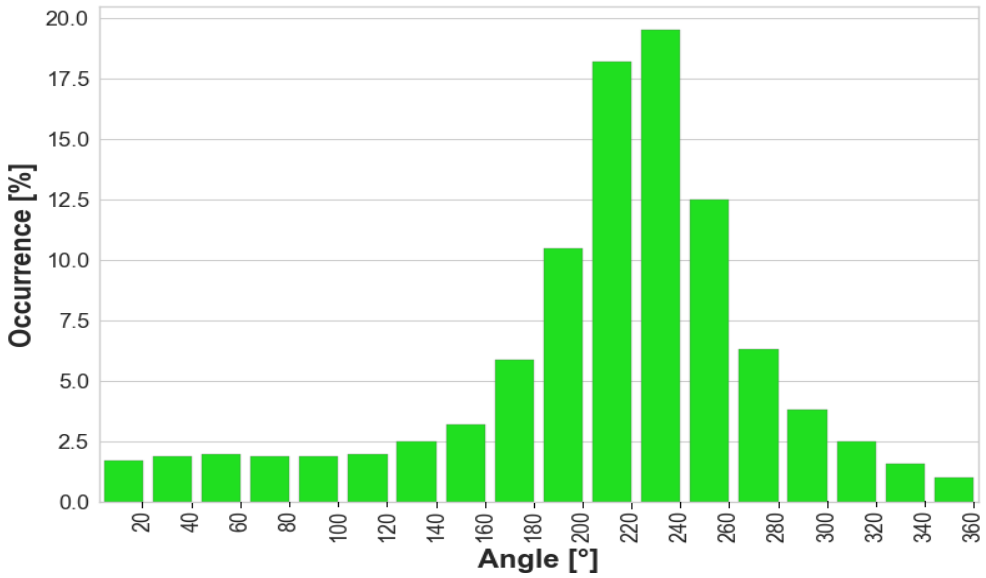

Figure 12. Same as Figure 11 but for the mean orientation.

Dessens (1986) found a mean length of 80 km for a small sample of 30 hailstorms in southwestern France. Note that Dessens (1986) used hail observations related to crop damage from the ANELFA network. For Spain, Mallafré et al. (2009) determined a mean hailstreak length of around 50 $\pm$ 20 km **and used the Storm Cell Identification and Tracking algorithm (SCIT) elaborated by Johnson et al. (1998) on 3D radar data over northern Spain during 2004 and 2005 in order to identify hail cells.**

The distribution of the hail track duration ~~**occurrence rate of hail track durations**~~ (Figure 11) is in accordance with the length, and also decreases almost exponentially with a peak at 30 minutes ~~**(not shown)**~~. As for the other physical characteristics, long-lived swaths are rare: only 2.4% of all cells persist over 5 hours (Fluck, 2018). The width, expressed as the maximum diameter of the largest reflectivity core ($Z \geq 55$ dBZ) during a hailstorm, or the longest distance between two cores evolving laterally in cases of cell-merging or splitting, show approximately a Gaussian distribution. The peak is between 9 and 10 km (41% of all events; not shown). However, as only the largest width of each swath is recorded, the results may be overestimated.

The track angle shown in Figure 12 represents the mean orientation of a storm track, and is the angle recorded by CCTA2D at the center of a swath, as most of the storm tracks are approximately linear. The orientation is defined as the angle between the line intersecting the reflectivity core centers, before and after the central point of a swath, and the parallel of latitude intersecting the start point. With this method, three time steps (i.e., 10 minutes) must exist for a track to be recorded. The maximum occurrence (19.3%) is found in the propagation direction between 220 and 240°, i.e., with a southwest direction. Around half (51%) of the hailstorms come from a west-southwest direction between 200 and 260°. Only 2.8% of the swaths

have a northwesterly direction. The principal southwesterly swath orientation found in the statistics confirmed previous results, such as that in the study of Puskeiler (2013), who found the highest number of hail days in southwest Germany with swaths oriented in southwesterly direction. In the Aquitaine region in France, Berthet et al. (2013) found that between 1952 and 1980 severe hailfalls came from a southwesterly direction with a mean angle of 241°.

5 Conclusions

This paper presents the first high resolution, radar-based hail statistics for a large central European region covering the countries of France, Germany, Belgium, and Luxembourg over a 10-year period. A European radar composite has been created from **French and German** national radar composites with a five minute time step and corrected with lightning data. Tracks of SCS have been reconstructed using the tracking algorithm CCTA2D. Only grid points exceeding the ~~**Mason**~~ Mason (1971) criterion for hail ($Z \geq 55$ dBZ) have been used for the hail assessment. From the spatial analyses of the hail signals, the following main results are obtained:

- The frequency of hailstorms shows a very large spatial variability across the investigation area. In general, there is a coast-to-continental increase in the number of hail days. While none or only several radar-derived hail days occurred in the northern parts of Germany, Brittany or along the European coastlines (0-2 hail days), the number of hail days far off the coasts is much higher.

- Most of the hail hot spots are found on the leeward side of low-mountain ranges such as the Massif Central in France or the Black Forest in Germany. The high spatial variability in the number of radar-derived hail days and the increasing number around orographic structures suggest a strong relationship between hailstorm occurrence and flow conditions induced or invigorated by ~~**to**~~ orography such as a flow-around regime with subsequence flow convergence on the lee side.

- On the regional-scale, significant differences in the seasonal and diurnal cycles of hail occurrences are found across Europe: In Southwest France, for instance, the hail maximum is in mid-June, but occurs two months later in August in eastern Germany.

Our radar-derived hail frequency estimations and maps have, of course, several limitations and uncertainties. First, due to the local-scale nature of hailstorms and the lack of accurate observations, the reconstructed streaks and their statistics are difficult to validate. No homogeneous monitoring system for hail exists over the entire investigation region, but only some local networks, for example, the hailpad network over the Southwest, Central, and Southern France operated by ANELFA are available. However, hailpad networks do not exist in Belgium, Luxembourg, and Germany. Thus, the use of radar and lightning data only **~~allows obtaining hail proxies~~ provides proxys for hail occurrence**. **~~In particular, 2D radar data does not consider the vertical extent of reflectivity cores or echotop height as provided by 3D radar data~~. Because only 2D radar data were available for this study, more sophisticated hail detection algorithm, such as those based on echo-top height (e.g. POH)**

or vertical integrals of reflectivity (e.g. MESH), which generally show higher skill in hail prediction (e.g.Skripniková and Řezáčová, 2014, Kunz and Kugel, 2015, Puskeiler et al., 2016), could not have been applied. The radar coverage over Western Europe is reliable, but several regions are still not or not sufficiently covered by several radars, such as the Alpine chain or some areas in the southeastern part of Germany and near Lake Constance. This leads to some data gaps in the final composite.

Despite the above mentioned limitations in our methods, the final results are in good accordance to other studies such as those for Germany based on 3D radar data (Puskeiler, 2013, Puskeiler et al., 2016, Schmidberger, 2018). The spatial distribution of hail signals in our study area is also similar to satellite-estimated hail frequency based on overshooting cloud tops as described by Punge et al. (2014) and Punge et al. (2017).

The investigations can be improved by extending the observation period until today. This is important especially in the subdomains highly exposed to hail. More accurate detections of hail can be achieved via the recently installed X-band radars in the French Alps. Furthermore, detailed investigations of the flow characteristics depending on atmospheric conditions, for example by using high-resolution numerical weather prediction models, can help to find robust evidence of the flow-around regime that may be decisive for the increased hail frequency downstream of several low mountain ranges, and can also contribute to a better understanding of the influence of orography on the triggering of convection.

Data availability. 2D radar data for Germany can be accessed via the German Weather Service (DWD) ftp server, while French national radar composites are available upon request to the French Meteorological Service (Météo-France). SCS/hail tracks were computed on radar data and are available upon request to M. Kunz. ERA5 data can be downloaded from the ECMWF server.

Author contributions. EF edited most parts of the paper, performed the statistical analyses and computed the SCS/hail tracks. MK verified in details the analytical methods and results, added crucial suggestions to the paper and contributed to the editing/revision of the manuscript. PG and SR added constructive suggestions to the paper. MK supervised the project in collaboration with PG and SR.

Competing interests. The authors declare that they have no conflict of interest.

Acknowledgements. The authors thank the French Meteorological Service (Météo-France) and the German Weather Service (DWD) for providing long-term radar data, and Siemens AG (S. Thern) for the supply of lightning data. The authors also acknowledge Tokio Millennium Re Ltd for funding the project. We acknowledge the constructive and very helpful comments from two anonymous reviewers that helped to improve the quality of this manuscript.

References

Amante, C. and Eakins, B. W.: ETOPO1 arc-minute global relief model: procedures, data sources and analysis, https://www.ngdc.noaa.gov/mgg/global/relief/ETOPO1/docs/ETOPO1.pdf, 2009.

Auer, A. H.: Distribution of graupel and hail with size, Mon. Wea. Rev., 100, 325–328, 1972.

Augros, C., Tabary, P., Anquez, A., Moisselin, J.-M., Brovelli, P., and Bousquet, O.: Development of a nationwide, low-level wind shear mosaic in France, Wea. Forecasting, 28, 1241–1260, https://doi.org//10.1175/WAF-D-12-00115.1, 2013.

Bartels, H., Weigl, E., Reich, T., Lang, P., Wagner, A., Kohler, O., and Gerlach, N.: Projekt RADOLAN–Routineverfahren zur Online-Aneichung der Radarniederschlagsdaten mit Hilfe von automatischen Bodenniederschlagsstationen (Ombrometer), Tech. rep., https://www.dwd.de/DE/leistungen/radolan/radolan_info/abschlussbericht_pdf.pdf?__blob=publicationFile&v=2, 2004.

Barthlott, C., Adler, B., Kalthoff, N., Handwerker, J., Kohler, M., and Wieser, A.: The role of Corsica in initiating nocturnal offshore convection, Q. J. R. Meteorol. Soc., 142, 222–237, https://doi.org//10.1002/qj.2415, 2016.

Bastin, S., Drobinski, P., Dabas, A., Delville, P., Reitebuch, O., and Werner, C.: Impact of the Rhône and Durance valleys on sea-breeze circulation in the Marseille area, Atmos. Res., 74, 303–328, https://doi.org//10.1016/j.atmosres.2004.04.014, 2005.

Baughman, R. and Fuquay, D.: Hail and lightning occurrence in mountain thunderstorms, J. Appl. Meteorol., 9, 657–660, https://doi.org//10.1175/1520-0450(1970)009<0657:HALOIM>2.0.CO;2, 1970.

Beck, J. and Bousquet, O.: Using gap-filling radars in mountainous regions to complement a national radar network: Improvements in multiple-Doppler wind syntheses, J. Appl. Meteor. Climatol., 52, 1836–1850, https://doi.org//10.1175/JAMC-D-12-0187.1, 2013.

Bedka, K.: Overshooting cloud top detections using MSG SEVIRI Infrared brightness temperatures and their relationship to severe weather over Europe, Atmos. Res., 99, 175–189, https://doi.org//10.1016/j.atmosres.2010.10.001, 2011.

Berthet, C., Dessens, J., and Sanchez, J. L.: Regional and yearly variations of hail frequency and intensity in France, Atmos. Res., 100, 391–400, https://doi.org//10.1016/j.atmosres.2010.10.008, 2011.

Berthet, C., Wesolek, E., Dessens, J., and Sanchez, J. L.: Extreme hail day climatology in Southwestern France, Atmos. Res., 123, 139–150, https://doi.org//10.1016/j.atmosres.2012.10.007, 2013.

Bousquet, O., Tabary, P., and Parent-du Châtelet, J.: Observation opérationnelle du vent 3D dans les nuages à partir des radars du réseau Aramis, La Météorologie, pp. 41–51, https://doi.org//10.4267/2042/17789, 2008.

Cantat, O.: Analyse critique sur les tendances pluviométriques au 20eme siècle en Basse-Normandie: Réfléxions sur la fiabilité des données et le changement climatique, Climatol., 1, 11–32, https://doi.org//10.4267/climatologie.963, 2004.

Caylor, I. and Chandrasekar, V.: Time-varying ice crystal orientation in thunderstorms observed with multiparameter radar, Trans. Geosci. Remote Sens., 34, 847–858, https://doi.org//10.1109/36.508402, 1996.

Chaboureau, J.-P., Chédin, A., and Scott, N. A.: Relationship between sea surface temperature, vertical dynamics, and the vertical distribution of atmospheric water vapor inferred from TOVS observations, Geophys. Res., 103, 23 173–23 180, https://doi.org//10.1029/98JD02019, 1998.

Champeaux, J., Laurantin, O., Mercier, B., Mounier, F., Lassegues, P., and Tabary, P.: Quantitative precipitation estimations using rain gauges and radar networks: inventory and prospects at Meteo-France, in: WMO Joint Meeting of CGS Expert Team on Surface-based Remotely-sensed Observations and CIMO Expert Team on Operational Remote Sensing, vol. 5, pp. 1–11, https://doi.org/https://www.wmo.int/pages/prog/www/OSY/Meetings/ET-SBRSO_ET-RSO-2011/DocPlan/INF.3.3.2_Report_METEOFRANCE_QPE.pdf, 2011.

Changnon, S. and Changnon, D.: Long-term fluctuations in hail incidences in the United States, J. Climate, 13, 658–664, http://journals.ametsoc.org/doi/abs/10.1175/1520-0442%282000%29013%3C0658%3ALTFIHI%3E2.0.CO%3B2, 2000.

Changnon, S. A.: The scales of hail, J. Appl. Meteorol., 16, 626–648, https://doi.org//10.1175/1520-0450(1977)016<0626:TSOH>2.0.CO;2, 1977.

Changnon, S. A.: Data and approaches for determining hail risk in the contiguous United States, J. Appl. Meteorol., 38, 1730–1739, https://doi.org//10.1175/1520-0450(1999)038<1730:DAAFDH>2.0.CO;2, 1999.

Chappell, C. F.: Quasi-stationary convective events, Springer, London, https://link.springer.com/chapter/10.1007/978-1-935704-20-1_13, 1986.

Cintineo, J. L., Smith, T. M., Lakshmanan, V., Brooks, H. E., and Ortega, K. L.: An objective high-resolution hail climatology of the contiguous United States, Wea. Forecasting, 27, 1235–1248, https://doi.org//10.1175/WAF-D-11-00151.1, 2012.

Damato, F., Planchon, O., and Dubreuil, V.: A remote-sensing study of the inland penetration of sea-breeze fronts from the English Channel, Weather, 58, 219–226, https://doi.org//10.1256/wea.50.02, 2003.

Dee, D., Uppala, S., Simmons, A., Berrisford, P., Poli, P., Kobayashi, S., Andrae, U., Balmaseda, M., Balsamo, G., Bauer, P., et al.: The ERA-Interim reanalysis: Configuration and performance of the data assimilation system, Quat. J. Roy. Meteor. Soc., 137, 553–597, 2011.

Deepen, J.: Schadenmodellierung extremer Hagelereignisse in Deutschland, Master's thesis, Institut für Landschaftsökologie der Westfälischen Wilhelms-Universität Münster, https://doi.org/https://www.uni-muenster.de/imperia/md/content/landschaftsoekologie/klima/pdf/2006_deepen_dipl.pdf, 2006.

Dessens, J.: Hail in Southwestern France. I: Hailfall Characteristics and Hailstrom Environment, J. Clim. Appl. Meteorol., 25, 35–47, https://doi.org//10.1175/1520-0450(1986)025<0035:HISFIH>2.0.CO;2, 1986.

Dessens, J., Berthet, C., and Sanchez, J.: Change in hailstone size distributions with an increase in the melting level height, Atmos. Res., 158, 245–253, https://doi.org//10.1016/j.atmosres.2014.07.004, 2015.

DeutscheRück: Sturmdokumentation 2012 Deutschland, Tech. rep., Deutsche Rückversicherung, https://www.deutscherueck.de/fileadmin/user_upload/WEB_Sturmdoku_2012.pdf, 2013.

Dimitrievski, V.: Characteristics of hail processes and hail falls in Macedonia, J. Weather Modif., 1, 62–63, http://www.journalofweathermodification.org/index.php/JWM/article/view/90/74, 1983.

Dotzek, N., Groenemeijer, P., Feuerstein, B., and Holzer, A. M.: Overview of ESSL's severe convective storms research using the European Severe Weather Database ESWD, Atmos. Res., 93, 575–586, https://doi.org//10.1016/j.atmosres.2008.10.020, 2009.

Doviak, R. J. and Zrnić, D. S.: Doppler radar and weather observations, Courier Corporation, https://doi.org/https://books.google.co.il/books/about/Doppler_Radar_and_Weather_Observations.html?id=ispLkPX9n2UCredir_esc=y, 2006.

Eccel, E., Cau, P., Riemann-Campe, K., and Biasioli, F.: Quantitative hail monitoring in an alpine area: 35-year climatology and links with atmospheric variables, Int. J. Climatol., 32, 503–517, 2012.

Figueras i Ventura, J. and Tabary, P.: The new French operational polarimetric radar rainfall rate product, J. Appl. Meteorol. Clim, 52, 1817–1835, https://doi.org//10.1175/JAMC-D-12-0179.1, 2013.

Figueras i Ventura, J., Boumahmoud, A.-A., Fradon, B., Dupuy, P., and Tabary, P.: Long-term monitoring of French polarimetric radar data quality and evaluation of several polarimetric quantitative precipitation estimators in ideal conditions for operational implementation at C-band, Q.J.R. Meteorol. Soc, 138, 2212–2228, https://doi.org//10.1002/qj.1934, 2012.

Fluck, E.: Hail statistics for European countries, Ph.D. thesis, Karlsruhe Institute of Technology, https://pdfs.semanticscholar.org/74b5/2e00fd4d299e40011d73aa596c6846212252.pdf, 2018.

Fouillet, A., Rey, G., Wagner, V., Laaidi, K., Empereur-Bissonnet, P., Le Tertre, A., Frayssinet, P., Bessemoulin, P., Laurent, F., De Crouy-Chanel, P., et al.: Has the impact of heat waves on mortality changed in France since the European heat wave of summer 2003? A study of the 2006 heat wave, Int. J. Epidem., 37, 309–317, https://doi.org//10.1093/ije/dym253, 2008.

Fraile, R., Castro, A., and Sánchez, J. L.: Analysis of hailstone size distributions from a hailpad network, Atmos. Res., 28, 311–326, https://doi.org//10.1016/0169-8095(92)90015-3, 1992.

Fraile, R., Berthet, C., Dessens, J., and Sánchez, J. L.: Return periods of severe hailfalls computed from hailpad data, Atmos. Res., 67, 189–202, https://doi.org//10.1016/S0169-8095(03)00051-6, 2003.

Glickman, T. and Walter, Z.: Glossary of Meteorology, Amer. Meteor. Soc.,, 2000.

Gourley, J. J., Tabary, P., and Parent du Chatelet, J.: Data quality of the Meteo-France C-band polarimetric radar, J. Atmos. Ocean. Technol., 23, 1340–1356, https://doi.org//10.1175/JTECH1912.1, 2006.

Gregg, W. and Tannehill, I.: International standard projections for meteorological charts, Mon. Wea. Rev., 65, 411–415, 1937.

Gudd, M.: Gewitter und Gewitterschäden im südlichen hessischen Berg-und Beckenland und im Rhein-Main-Tiefland 1881 bis 1980: eine Auswertung mit Hilfe von Schadensdaten, Ph.D. thesis, University of Mainz, https://publications.ub.uni-mainz.de/theses/volltexte/2004/523/pdf/523.pdf, 2003.

Handwerker, J.: Cell Tracking with TRACE3D: a New Algorithm, Atmos. Res., 61, 15–34, https://doi.org//10.1016/S0169-8095(01)00100-4, 2002.

Hermida, L., Sánchez, J. L., López, L., Berthet, C., Dessens, J., García-Ortega, E., and Merino, A.: Climatic trends in hail precipitation in France: spatial, altitudinal, and temporal variability, Sci. World. J., 2013, https://doi.org//10.1155/2013/494971, 2013.

Hermida, L., López, L., Merino, A., Berthet, C., García-Ortega, E., Sánchez, J. L., and Dessens, J.: Hailfall in Southwest France: Relationship with precipitation, trends and wavelet analysis, Atmos. Res., 156, 174–188, https://doi.org//10.1016/j.atmosres.2015.01.005, 2015.

Hersbach, H., Bell, B., Berrisford, P., Hirahara, S., Horányi, A., Muñoz-Sabater, J., Nicolas, J., Peubey, C., Radu, R., Schepers, D., et al.: The ERA5 global reanalysis, Q. J. R. Meteorol. Soc., https://doi.org//10.1002/qj.3803, 2020.

Hohl, R.: Relationship between hailfall intensity and hail damage on ground, determined by radar and lightning observations, Ph.D. thesis, Departement of Geography, University of Fribourg, Switzerland, https://doc.rero.ch/record/5136/files/1_HohlRM.pdf, 2001.

Hohl, R., Schiesser, H.-H., and Aller, D.: Hailfall: the relationship between radar-derived hail kinetic energy and hail damage to buildings, Atmos. Res., 63, 177–207, https://doi.org//10.1016/S0169-8095(02)00059-5, 2002.

Holton, J. R.: An introduction to dynamic meteorology, Academic press, San Diego, 2004.

Houze J, R. A.: Cloud dynamics, Academic press, https://www.sciencedirect.com/bookseries/international-geophysics/vol/104/suppl/C, 2014.

Huschke, R. E.: Glossary of meteorology, American Meteorological Society, 1959.

Jenkner, J., Sprenger, M., Schwenk, I., Schwierz, C., Dierer, S., and Leuenberger, D.: Detection and climatology of fronts in a high-resolution model reanalysis over the Alps, Q. J. R. Meteorol.Soc., 17, 1–18, https://doi.org//10.1002/met.142, 2010.

Johnson, J., MacKeen, P. L., Witt, A., Mitchell, E. D. W., Stumpf, G. J., Eilts, M. D., and Thomas, K. W.: The storm cell identification and tracking algorithm: An enhanced WSR-88D algorithm, Wea. Forecasting, 13, 263–276, https://doi.org/10.1175/1520-0434(1998)013<0263:TSCIAT>2.0.CO;2, 1998.

Junghänel, T., Brendel, C., Winterrath, T., and Walter, A.: Towards a radar- and observation-based hail climatology for Germany, Meteorol. Z., 25, 435–445, https://doi.org/10.1127/metz/2016/0734, 2016.

Kaltenböck, R., Diendorfer, G., and Dotzek, N.: Evaluation of thunderstorm indices from ECMWF analyses, lightning data and severe storm reports, Atmos. Res., 93, 381–396, https://doi.org//10.1016/j.atmosres.2008.11.005, 2009.

Kirshbaum, D. J., Adler, B., Kalthoff, N., Barthlott, C., and Serafin, S.: Moist orographic convection: Physical mechanisms and links to surface-exchange processes, Atmosphere, 9, 80, https://doi.org/https://doi.org/10.3390/atmos9030080, 2018.

Koebele, D.: Analyse von Konvergenzbereichen bei Hagelereignissen stromab von Mittelgebirgen anhand von COSMO-Modellsimulationen, Master's thesis, Karlsruhe Institute of Technology, https://www.imk-tro.kit.edu/download/Masterarbeit_Koebele.pdf, 2014.

Kreklow, J., Tetzlaff, B., Burkhard, B., and Kuhnt, G.: Radar-Based Precipitation Climatology in Germany—Developments, Uncertainties and Potentials, Atmosphere, 11, 217, https://doi.org//10.3390/atmos11020217, 2020.

Kunz, M.: The skill of convective parameters and indices to predict isolated and severe thunderstorms, Nat. Hazards Earth Syst. Sci., 7, 327–342, https://doi.org/https://doi.org/10.5194/nhess-7-327-2007,, 2007.

Kunz, M. and Kugel, P. I.: Detection of hail signatures from single-polarization C-band radar reflectivity, Atmos. Res., 153, 565–577, https://doi.org//10.1016/j.atmosres.2014.09.010, 2015.

Kunz, M. and Puskeiler, M.: High-resolution Assessment of the Hail Hazard over Complex Terrain from Radar and Insurance Data, Meteorol. Z., 19, 427–439, https://doi.org//10.1127/0941-2948/2010/0452, 2010.

Kunz, M., Blahak, U., Handwerker, J., Schmidberger, M., Punge, H. J., Mohr, S., Fluck, E., and Bedka, K. M.: The severe hailstorm in SW Germany on 28 July 2013: Characteristics, impacts, and meteorological conditions, Q. J. R. Meteorol. Soc., 144, 231–250, https://doi.org//10.1002/qj.3197, 2018.

Kunz, M., Wandel, J., Fluck, E., Baumstark, S., Mohr, S., and Schemm, S.: Ambient conditions prevailing during hail events in central Europe, Natural Hazards and Earth System Sciences, 20, 1867–1887, https://doi.org//10.5194/nhess-20-1867-2020, 2020.

Langhans, W., Schmidli, J., Fuhrer, O., Bieri, S., and Schär, C.: Long-term simulations of thermally driven flows and orographic convection at convection-parameterizing and cloud-resolving resolutions, J. Appl. Meteor., 52, 1490–1510, 2013.

Lenderink, G., Van Meijgaard, E., and Selten, F.: Intense coastal rainfall in the Netherlands in response to high sea surface temperatures: analysis of the event of August 2006 from the perspective of a changing climate, Clim. Dyn., 32, 19–33, https://doi.org/10.1007/s00382-008-0366-x, 2009.

Ligda, M. G.: The radar observation of lightning, J. Atmos. Terr. Phys., 9, 309–346, https://doi.org//10.1016/0021-9169(56)90152-0, 1956.

Ludlam, F. H.: Clouds and storms: The behavior and effect of water in the atmosphere, Pennsylvania State University Press, http://agris.fao.org/agris-search/search.do?recordID=US8025686, 1980.

Lukach, M. and Delobbe, L.: Radar-based hail statistics over Belgium, in: 7th European Conference on Severe Storms (ECSS), 7-13 June 2013, Helsinki, Finland, 2013.

Lukach, M., Foresti, L., Giot, O., and Delobbe, L.: Estimating the occurrence and severity of hail based on 10 years of observations from weather radar in Belgium, Meteorol. Appl., 24, 250–259, https://doi.org//10.1002/met.1623, 2017.

Mallafré, M. C., Ribas, T. R., del Carmen Llasat Botija, M., and Sánchez, J. L.: Improving hail identification in the Ebro Valley region using radar observations: Probability equations and warning thresholds, Atmos. Res., 93, 474–482, https://doi.org//10.1016/j.atmosres.2008.09.039, 2009.

Markowski, P. and Richardson, Y.: Mesoscale meteorology in midlatitudes, vol. 3, John Wiley, https://onlinelibrary.wiley.com/doi/book/10.1002/9780470682104, 2010.

Martín, J. A. G., Hijano, C. F., Jara, J. C. M., Cardineau, C. A., Fernández, A. F., and Piserra, M. T.: Tormentas con pedrisco en Castilla-La Mancha: estudio sobre los eventos de granizo en el periodo 1850-1950 y desarrollo de una base de datos y su implantación en un SIG aplicado a la región, Segur. Medio. Ambi., pp. 32–45, https://www.fundacionmapfre.org/documentacion/publico/i18n/catalogo_imagenes/grupo.cmd?path=1062523, 2010.

Mason, B.: The physics of clouds, Oxford University Press, Oxford, https://doi.org//10.1002/qj.49709841723, 1971.

Mass, C.: Topographically forced convergence in western Washington State, Monthly Weather Review, 109, 1335–1347, https://doi.org//10.1175/1520-0493(1981)109<1335:TFCIWW>2.0.CO;2, 1981.

Merino, A., García-Ortega, E., López, L., Sánchez, J., and Guerrero-Higueras, A.: Synoptic environment, mesoscale configurations and forecast parameters for hailstorms in Southwestern Europe, Atmos. Res., 122, 183–198, https://doi.org//10.1016/j.atmosres.2012.10.021, 2013.

Mohr, S. and Kunz, M.: Recent trends and variabilities of convective parameters relevant for hail events in Germany and Europe, Atmos. Res., 123, 211–228, https://doi.org//10.1016/j.atmosres.2012.05.016, 2013.

Mohr, S., Kunz, M., and Geyer, B.: Hail potential in Europe based on a regional climate model hindcast, Geophys. Res. Lett., 42, 10 904–10 912, https://doi.org/doi:10.1002/2015GL067118., 2015a.

Mohr, S., Kunz, M., and Keuler, K.: Development and application of a logistic model to estimate the past and future hail potential in Germany, J. Geophys. Res., 120, 3939–3956, https://doi.org/10.1002/2014JD022959, 2015b.

Mohr, S., W. J. L. S. and Martius, O.: Relationship between atmospheric blocking and warm-season thunderstorms over western and central Europe, Q. J. Roy. Meteorol. Soc., 145, 3040–3056, https://doi.org//10.1002/qj.3603, 2019.

Morgan, G. M.: A general description of the hail problem in the Po Valley of northern Italy, J. Appl. Meteorol., 12, 338–353, https://doi.org/10.1175/1520-0450(1973)012<0338:AGDOTH>2.0.CO;2, 1973.

Morris, R.: The Spanish plume-testing the forecasters nerve, Meteorol. Mag., 115, 349–357, 1986.

Nesbitt, S. W. and Zipser, E. J.: The diurnal cycle of rainfall and convective intensity according to three years of TRMM measurements, J. Clim, 16, 1456–1475, https://doi.org/10.1175/1520-0442(2003)016<1456:TDCORA>2.0.CO;2, 2003.

Nisi, L., Ambrosetti, P., and Clementi, L.: Nowcasting severe convection in the Alpine region: The COALITION approach, Q. J. R. Meteorol. Soc., 140, 1684–1699, https://doi.org//10.1002/qj.2249, 2014.

Nisi, L., Martius, O., Hering, A., Kunz, M., and Germann, U.: Spatial and temporal distribution of hailstorms in the Alpine region: a long-term, high resolution, radar-based analysis, Q. J. R. Meteorol. Soc., 142, 1590–1604, https://doi.org//10.1002/qj.2771, 2016.

Nisi, L., Hering, A., Germann, U., and Martius, O.: A 15-year hail streak climatology for the Alpine region, Q. J. R. Meteorol. Soc., 144, 1429–1449, https://doi.org//10.1002/qj.3286, 2018.

NOAA: Global Climate Report for Annual 2006, Tech. rep., NOAA National Centers for Environmental Information, https://www.ncdc.noaa.gov/sotc/global/200713, 2007.

NOAA: Global Climate Report for Annual 2010, Tech. rep., National Centers for Environmental Information, https://www.ncdc.noaa.gov/sotc/global/201013, 2011.

Parent du Châtelet, J., Tabary, P., and Lamarque, P.: Evolution du réseau radar opérationnel de Météo-France pour une meilleure estimation des lames d'eau, Hydrol. Cont., 49, 1–4, 2005.

Pilorz, W. and Łupikasza, E.: Radar reflectivity signatures and possible lead times of warnings for very large hail in Poland based on data from 2007-2015, Environ. Socio.-econ. Stud, 8, 34–47, https://doi.org//10.2478/environ-2020-0016, 2020.

Piper, D. and Kunz, M.: Spatiotemporal variability of lightning activity in Europe and the relation to the North Atlantic Oscillation teleconnection pattern., Nat. Hazards Earth Syst. Sci., 17, https://doi.org//10.5194/nhess-17-1319-2017, 2017.

Piper, D. A.: Untersuchung der Gewitteraktivität und der relevanten großräumigen Steuerungsmechanismen über Mittel- und Westeuropa, Ph.D. thesis, Karlsruhe Institute of Technology, https://doi.org/doi:10.5445/KSP/1000072089, 2017.

Piper, D. A., Kunz, M., Allen, J. T., and Mohr, S.: Investigation of the temporal variability of thunderstorms in Central and Western Europe and the relation to large-scale flow and teleconnection patterns, Q. J. R. Meteorol. Soc., 145, 3644–3666, https://doi.org//10.1002/qj.3647, 2019.

Pohjola, H. and Mäkelä, A.: The comparison of GLD360 and EUCLID lightning location systems in Europe, Atmos. Res., 123, 117–128, https://doi.org//10.1016/j.atmosres.2012.10.019, 2013.

Punge, H. and Kunz, M.: Hail observations and hailstorm characteristics in Europe: A review, Atmos. Res., 176, 159–184, https://doi.org//10.1016/j.atmosres.2016.02.012, 2016.

Punge, H., Bedka, K., Kunz, M., and Werner, A.: A new physically based stochastic event catalog for hail in Europe, Nat. Hazards, 73, 1625–1645, https://doi.org//10.1007/s11069-014-1161-0, 2014.

Punge, H., Bedka, K., Kunz, M., and Reinbold, A.: Hail frequency estimation across Europe based on a combination of overshooting top detections and the ERA-INTERIM reanalysis, Atmos. Res., 198, 34–43, https://doi.org/doi:10.1016/j.atmosres.2017.07.025, 2017.

Punkka, A.-J. and Bister, M.: Occurrence of summertime convective precipitation and mesoscale convective systems in Finland during 2000–01, Mon. Wea. Rev., 133, 362–373, https://doi.org//10.1175/MWR-2854.1, 2005.

Puskeiler, M.: Radarbasierte Analyse der Hagelgefährdung in Deutschland, Ph.D. thesis, Karlsruhe Institute of Technology, http://www.imk-tro.kit.edu/download/Dissertation_Puskeiler_Marc.pdf, 2013.

Puskeiler, M., Kunz, M., and Schmidberger, M.: Hail statistics for Germany derived from single-polarization radar data, Atmos. Res., 178, 459–470, https://doi.org//10.1016/j.atmosres.2016.04.014, 2016.

Queney, P.: The problem of air flow over mountains:{A} summary of theoretical studies, Bull. Am. Meteorol. Soc., 29, 16–26, https://doi.org//10.1175/1520-0477-29.1.16, 1948.

Rädler, A. T., Groenemeijer, P., Faust, E., and Sausen, R.: Detecting Severe Weather Trends Using an Additive Regressive Convective Hazard Model (AR-CHaMo), J. Appl. Meteorol., 57, 569–587, https://doi.org//10.1175/JAMC-D-17-0132.1, 2018.

Schemm, S., Nisi, L., Martinov, A., Leuenberger, D., and Martius, O.: On the link between cold fronts and hail in Switzerland, Atmos. Sci. Lett, 17, 315–325, 2016.

Schmidberger, M.: Hagelgefährdung und Hagelrisiko in Deutschland basierend auf einer Kombination von Radardaten und Versicherungsdaten, phdthesis, Karlsruhe Institute of Technology, https://doi.org/doi:10.5445/KSP/1000086012, 2018.

Schulz, W., Diendorfer, G., Pedeboy, S., and Poelman, D. R.: The European lightning location system EUCLID–Part 1: Performance analysis and validation, Nat. Hazards Earth Syst. Sci, 16, 595–605, 2016.

Schuster, S. S., Blong, R. J., and Speer, M. S.: A hail climatology of the greater Sydney area and New South Wales, Australia, Int. J. Climatol., 25, https://doi.org//10.1002/joc.1199, 2005.

Simpson, J. E.: Sea breeze and local winds, Cambridge University Press, Cambridge, https://books.google.co.il/books?hl=en&lr=&id=6WPodgtunqIC&oi=fnd&pg=PP17&dq=Simpson,+J.+E.,+1994:Sea+breeze+and+local+winds.+Cambridge+University+Press,+Cambridge,+239+pp&ots=Erev75mbTE&sig=I_BqDmgDoAFfa3stgrHYZHW_Li0&redir_esc=y#v=onepage&q&f=false, 1994.

Skripniková, K. and Řezáčová, D.: Radar-based hail detection, Atmos. Res., 144, 175–185, https://doi.org/https://doi.org/10.1016/j.atmosres.2013.06.002, 2014.

Smith, R. B.: The influence of mountains on the atmosphere, in: Advances in Geophysics, vol. 21, pp. 87–230, 1979.

Smolarkiewicz, P. K. and Rotunno, R.: Low Froude number flow past three-dimensional obstacles. Part I: Baroclinically generated lee vortices, Journal of the Atmospheric Sciences, 46, 1154–1164, https://doi.org//10.1175/1520-0469(1989)046<1154:LFNFPT>2.0.CO;2, 1989.

Steiner, M. and Smith, J. A.: Use of three-dimensional reflectivity structure for automated detection and removal of nonprecipitating echoes in radar data, J. Atmos. Ocean. Technol, 19, 673–686, https://doi.org//10.1175/1520-0426(2002)019<0673:UOTDRS>2.0.CO;2, 2002.

Steppeler, J., Doms, G., Schättler, U., Bitzer, H. W., Gassmann, A., Damrath, U., and Gregoric, G.: Meso-gamma scale forecasts using the nonhydrostatic model LM, Meteorol. Atmos. Phys., 82, 75–96, https://doi.org/10.1007/s00703-001-0592-9, http://www.springerlink.com/content/wf867ehyemg1v4kb/, 2003.

SwissRe: Sigma: Natural- and Man-made Catastrophes 2013, Tech. rep., Swiss Re Economic Research and Consulting, https://reliefweb.int/sites/reliefweb.int/files/resources/SwisRe_2014_Natural_Catastrophes_sigma1_2014_en.pdf, 2014.

Tabary, P.: The new French operational radar rainfall product. Part I: Methodology, Wea. Forecasting, 22, 393–408, https://doi.org//10.1175/WAF1004.1, 2007.

Tabary, P., Guibert, F., Perier, L., and Parent-du Chatelet, J.: An operational triple-PRT Doppler scheme for the French radar network, J. Atmos. Ocean. Technol., 23, 1645–1656, https://doi.org//10.1175/JTECH1923.1, 2006.

Tabary, P., Augros, C., Champeaux, J.-L., Chèze, J.-L., Faure, D., Idziorek, D., Lorandel, R., Urban, B., and Vogt, V.: Le réseau et les produits radars de Météo-France, La Météorologie, pp. 15–27, https://doi.org//10.4267/2042/52050, 2013.

Twardosz, R., Niedzwiedz, T., and Lupikasza, E.: Hail thunderstorms in Cracow and their circulation determinants (1863–2008), W. Geograph. Res. University of Kielce, Kielce, pp. 295–305, http://komhydptg.geo.uni.lodz.pl/uploads/images/publikacje/kielce%202010.pdf, 2010.

Varga, J.: The Lambert conformal conic projection, Periodica Polytechnica Civil Engineering, 34, 153–158, https://doi.org/https://pp.bme.hu/ci/article/view/3899/3004, 1990.

Vinet, F.: Climatology of hail in France, Atmos. Res., 56, 309–323, https://doi.org//10.1016/S0169-8095(00)00082-X, 2001.

Vinet, F.: La question du risque climatique en agriculture: le cas de la grêle en France/Climatic risk in agriculture: the case of hail falls in France, in: Ann. Géograph., pp. 592–613, JSTOR, www.jstor.org/stable/23455979, 2002.

Waldvogel, A., Federer, B., and Grimm, P.: Criteria for the detection of hail cells, J. Appl. Meteorol., 18, 12, https://doi.org//10.1175/1520-0450(1979)018<1521:CFTDOH>2.0.CO;2, 1979.

Wapler, K.: The life-cycle of hailstorms: Lightning, radar reflectivity and rotation characteristics, Atmos. Res., 193, 60–72, https://doi.org/http://doi.org/10.1016/j.atmosres.2017.04.009, 2017.

Warren, R. A., Ramsay, H. A., Siems, S. T., Manton, M. J., Peter, J. R., Protat, A., and Pillalamarri, A.: Radar-based climatology of damaging hailstorms in Brisbane and Sydney, Australia, Q. J. R. Meteorol. Soc., 146, 505–530, https://doi.org//10.1002/qj.3693, 2020.

Weissmann, M., Braun, F. J., Gantner, L., Mayr, G. J., Rahm, S., and Reitebuch, O.: The Alpine mountain–plain circulation: Airborne Doppler lidar measurements and numerical simulations, Mon. Weather. Rev., 133, 3095–3109, https://doi.org//10.1175/MWR3012.1, 2005.

Wernli, H., Pfahl, S., Trentmann, J., and Zimmer, M.: How representative were the meteorological conditions during the COPS field experiment in summer 2007?, Meteorol. Z, 19, 619–630, https://doi.org//10.1127/0941-2948/2010/0483, 2010.

Yu, N., Gaussiat, N., and Tabary, P.: Polarimetric X-band weather radars for quantitative precipitation estimation in mountainous regions, Q. J. R. Meteorol. Soc., 144, 2603–2619, https://doi.org//10.1002/qj.3366, 2018.